Volume 45 | Number 35 | 21 September 2016 | Pages 13617–13980

Dalton Transactions

An international journal of inorganic chemistry

www.rsc.org/dalton

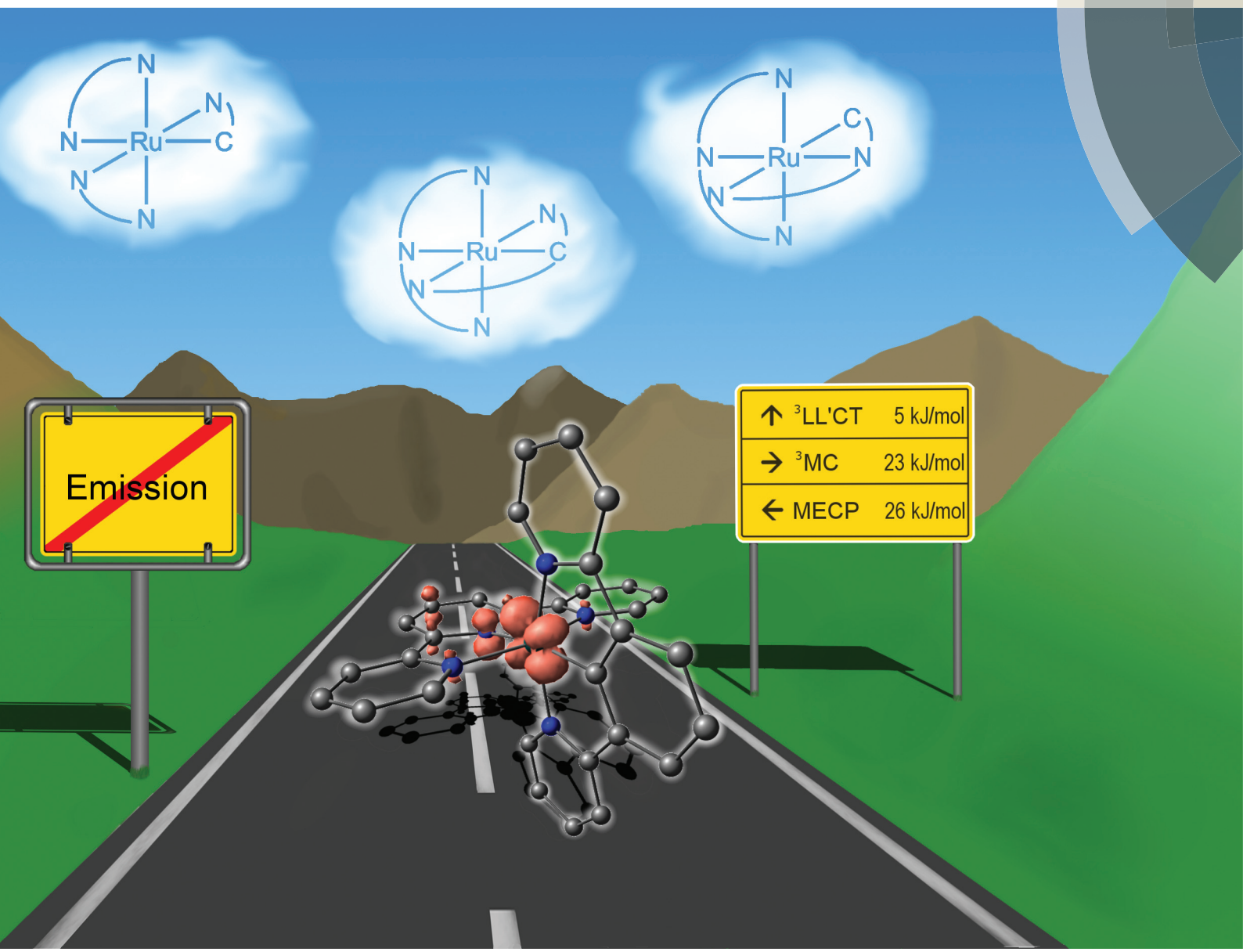

ISSN 1477-9226

ROYAL SOCIETY OF CHEMISTRY

PERSPECTIVE
Christoph Kreitner and Katja Heinze
Excited state decay of cyclometalated polypyridine ruthenium complexes: insight from theory and experiment

175 YEARS

Dalton Transactions

PERSPECTIVE

View Article Online
View Journal | View Issue

Cite this: *Dalton Trans.*, 2016, **45**, 13631

Excited state decay of cyclometalated polypyridine ruthenium complexes: insight from theory and experiment†

Christoph Kreitner[a,b] and Katja Heinze*[a]

Deactivation pathways of the triplet metal-to-ligand charge transfer (^{3}MLCT) excited state of cyclometalated polypyridine ruthenium complexes with $[RuN_5C]^+$ coordination are discussed on the basis of the available experimental data and a series of density functional theory calculations. Three different complex classes are considered, namely with $[Ru(N^N)_2(N^C)]^+$, $[Ru(N^N^N)(N^C^N)]^+$ and $[Ru(N^N^N)(N^N^C)]^+$ coordination modes. Excited state deactivation in these complex types proceeds *via* five distinct decay channels. Vibronic coupling of the ^{3}MLCT state to high-energy oscillators of the singlet ground state (^{1}GS) allows tunneling to the ground state followed by vibrational relaxation (path **A**). A ligand field excited state (^{3}MC) is thermally accessible *via* a ^{3}MLCT → ^{3}MC transition state with the ^{3}MC state being strongly coupled to the ^{1}GS surface *via* a low-energy minimum energy crossing point (path **B**). Furthermore, a ^{3}MLCT → ^{1}GS surface crossing point directly couples the triplet and singlet potential energy surfaces (path **C**). Charge transfer states either with higher singlet character or with different orbital parentage and intrinsic symmetry restrictions are thermally populated which promote non-radiative decay *via* tunneling to the ^{1}GS state (path **D**). Finally, the excited state can decay *via* phosphorescence (path **E**). The dominant deactivation pathways differ for the three individual complex classes. The implications of these findings for isoelectronic iridium(III) or iron(II) complexes are discussed. Ultimately, strategies for optimizing the emission efficiencies of cyclometalated polypyridine complexes of d^6-metal ions, especially Ru^{II}, are suggested.

Received 18th May 2016,
Accepted 16th June 2016

DOI: 10.1039/c6dt01989g

www.rsc.org/dalton

Introduction

Polypyridine complexes of a wide range of transition metals have received great interest from coordination chemists and materials scientists over the last few decades due to their versatile applicability. For example, such complexes of copper(I),[1–3] iron(II),[4–6] osmium(II),[7,8] iridium(III)[9,10] and, particularly, ruthenium(II)[11–19] were successfully applied as sensitizers in dye sensitized solar cells. Additionally, a wide range of complexes of this type have been successfully used as sensitizers in photoredox catalysis.[20–31]

Moreover, the most fascinating and thoroughly studied property observed for a large number of polypyridine transition metal complexes is their luminescence.[32,33] The first polypyridine complex reported to exhibit luminescence was $[Ru(bpy)_3]^{2+}$ (bpy = 2,2′-bipyridine).[34] Since then, luminescent polypyridine complexes have been described for second and third row transition metal ions with d^6, d^8 and d^{10} electron configuration,[35–37] namely for rhenium(I),[38–41] osmium(II),[42–45] rhodium(III),[46–48] iridium(III),[41,42,49–51] palladium(II),[52] platinum(II),[52–57] and gold(III).[58,59] Even a few luminescent first row transition metal polypyridine complexes are known of chromium(III),[60–64] copper(I)[65–71] and zinc(II).[72]

As such luminescence was first observed for ruthenium, most of the effort understanding the underlying electronic processes evolved around this element and in particular around $[Ru(bpy)_3]^{2+}$ as the prototype.[73–75] Its key features are an electron-rich low-spin d^6 metal center with $(t_{2g})^6$ electron configuration in idealized O_h symmetry and strongly π-accepting chelate ligands. Upon irradiation with visible light (λ_{max} = 452 nm),[73] $[Ru(bpy)_3]^{2+}$ is excited into its lowest excited singlet state which has metal-to-ligand charge transfer (MLCT) character.[76–78] As MLCT transitions are not restricted in terms of parity selection rules, the corresponding absorption bands are typically very intense. Due to the spin–orbit coupling induced by the ruthenium atom, the excited ^{1}MLCT state

[a]*Institute of Inorganic and Analytical Chemistry, Johannes Gutenberg University, Duesbergweg 10-14, D-55128 Mainz, Germany. E-mail: katja.heinze@uni-mainz.de*
[b]*Graduate School Materials Science in Mainz, Staudingerweg 9, D-55128 Mainz, Germany*

† Electronic supplementary information (ESI) available: DFT optimized Cartesian coordinates of the ^{1}GS and all relevant triplet states of complexes $[\mathbf{1b}]^+$, $[\mathbf{4a}]^+$ and $[\mathbf{7a}]^+$. See DOI: 10.1039/c6dt01989g

undergoes very efficient intersystem crossing ($\phi_{ISC} \approx 1$) onto the triplet hypersurface populating a ^{3}MLCT state.[79,80] At low temperatures in solid matrix, this state either evolves into the ground state without emission *via* tunnelling to the singlet energy surface and vibrational cooling or *via* phosphorescent emission of a photon (at 77 K: λ_{em} = 580 nm,[77] ϕ_{em} = 0.38;[77] at 298 K: λ_{em} = 621 nm,[81] ϕ_{em} = 0.095 [81]).[77,82–84] The rate of non-radiative excited state decay is hereby governed by the so-called energy gap law.[85–88] In a series of structurally related compounds, the rate increases with decreasing exited state energy. At room temperature however, a third deactivation pathway *via* metal centered (MC) d–d excited states ($(t_{2g})^5(e_g)^1$ electron configuration) is thermally accessible dramatically quenching the emission.[84,89–91] The activation barrier for this thermally activated depopulation was determined to be about 45 kJ mol^{-1} for $[Ru(bpy)_3]^{2+}$.[90,91]

This general scheme for $[Ru(bpy)_3]^{2+}$ is applicable to other ruthenium polypyridine complexes as well. It enables a fine-tuning of their emissive properties by manipulation of the ^{3}MLCT energies *via* introduction of functional groups or extension of the aromatic backbone of the pyridine ligands.[75,92–96] This allowed the design of specifically tailored complexes for luminescent sensing applications[97,98] and for optoelectronics.[99–102]

The concept was successfully transferred to polypyridine complexes of other transition metals. For example, cyclometalated polypyridine complexes of iridium(III) proved to be exceptionally well suited for PHOLED applications as their room temperature emission is typically very intense and can be tuned throughout the visible range of the electromagnetic spectrum.[41,103–106] Cyclometalation hereby refers to the exchange of one or multiple nitrogen atoms of the polypyridine's coordination sphere by isoelectronic carbon anions. This substitution typically yields a reduction of the overall charge of the complex moiety as well as a substantial shift of all redox processes to lower potentials.

Due to the fact that the isoelectronic cyclometalated complexes of ruthenium(II) perform very well as sensitizers in dye sensitized solar cells, they have also received increasing interest in the last years.[16,17,19,107–109] Additionally, cyclometalated bridging ligands enhance the electronic coupling between the redox centers in mixed-valent Ru/Ru complexes[110–112] and Ru/organic hybrid structures.[113–116] Despite the large variety of cyclometalated polypyridine ruthenium complexes synthesized up-to-date, however, no phosphorescence comparable to $[Ru(bpy)_3]^{2+}$ has yet been achieved. Furthermore, a general explanation for the striking difference in the luminescence

Christoph Kreitner

Christoph Kreitner is currently working on his PhD thesis in the research group of Prof. Dr Katja Heinze at the Johannes Gutenberg-University in Mainz, Germany (since 2013). There, his research focusses on the synthesis and understanding of new cyclometalated ruthenium complexes and their application in dye-sensitized solar cells. He studied chemistry at the Johannes Gutenberg-University in Mainz, Germany where he received his diploma degree in 2012. During his studies he spent one semester at the University of Toronto, Toronto, Canada (2010/2011), working in the Department of Inorganic Chemistry in the group of Prof. Douglas W. Stephan on Frustrated Lewis Pairs and their reactions with lactones and lactide. For his PhD thesis, he received a scholarship of the Graduate School of Excellence "Materials Science in Mainz" (2013) and became junior member of the Gutenberg Academy of the Johannes Gutenberg-University Mainz, Germany (2014). His research interests particularly aim at the understanding of electron and energy transfer as well as optoelectronic mechanisms in molecular systems.

Katja Heinze

Katja Heinze is professor of organometallic and bioinorganic chemistry at the Johannes Gutenberg-University of Mainz, Germany. After receiving a diploma degree (1995) and a Ph.D. degree (1998) from the Ruprecht Karls University of Heidelberg, Germany (G. Huttner), she went for a postdoctoral stay to the University of Zurich, Zurich, Switzerland (1999). She was appointed Privatdozent in 2004 at the University of Heidelberg, Germany, and Full Professor in 2008 at the Johannes Gutenberg-University of Mainz, Germany. She received the Lieseberg award of the Faculty of Chemistry and Earth Sciences, University of Heidelberg (2002), the Heisenberg fellowship from the Deutsche Forschungsgemeinschaft (2004), the Hengstberger Award of the University of Heidelberg (2007) and the Interregional Research Price of the Greater Region (2014). Currently she serves as chair of the Institute of Inorganic Chemistry and Analytical Chemistry, University of Mainz. From 2011 to 2015 she has served as a member of the International Advisory Board of Organometallics. Her key research interests comprise functional complex systems based on coordination and organometallic compounds with special emphasis on molecular wires, light-harvesting systems, bistable systems, emitters, switches and sensors as well as on (biomimetic) catalysts. She has authored more than 130 international refereed papers.

properties between the isoelectronic cyclometalated complexes of iridium(III) and ruthenium(II) is still missing.[117–119]

Hence, this issue will be addressed in this perspective. We will discuss the excited state deactivation processes of cyclometalated polypyridine complexes beyond the ^{3}MLCT/^{3}MC and energy gap law schemes by picking illustrative examples from the literature and elaborate why these are weak emitters at room temperature. Several decay pathways of the emissive ^{3}MLCT state are known for polypyridine ruthenium complexes, and their individual contribution to the excited state decay of cyclometalated polypyridine ruthenium complexes will be discussed (Fig. 1):

Decay path **A**: tunneling into high-lying vibrational levels of the singlet state.[86–88] This channel is always available and its efficiency depends on the Franck–Condon overlap of the vibrational wavefunctions of the ^{3}MLCT and singlet ground states (^{1}GS).

Decay path **B**: *via* a thermally accessible ^{3}MC state. Population of this state is followed by rapid surface crossing to the singlet potential energy surface *via* a close-lying minimum energy crossing point (MECP) and vibrational cooling.[56] The energy of the ^{3}MC state mainly depends on the ligand field strength.

Decay path **C**: direct surface crossing from the ^{3}MLCT state to the singlet potential surface *via* a low-lying surface crossing point. The energy of this MECP depends on the degree of ^{3}MLCT state distortion and the energy of the ^{3}MLCT state itself. A shallow ^{3}MLCT state potential surface around the minimum favours the occurrence of a surface crossing.

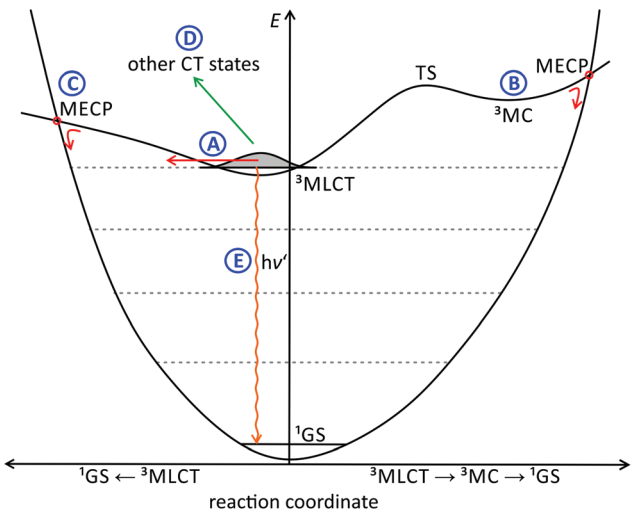

Fig. 1 Schematic representation of the energy landscape of a polypyridine ruthenium complex including all relevant deactivation pathways of an emissive ^{3}MLCT state: (A) tunneling into high-energy vibrationally excited singlet states; (B) thermally activated decay into a ^{3}MC state followed by surface crossing at a minimum energy crossing point (MECP), (C) direct thermally activated surface crossing from the ^{3}MLCT state to the singlet ground state, (D) decay *via* non-emissive charge transfer states, and (E) phosphorescence.

Decay path **D**: *via* other non-emissive triplet states or states with higher singlet character as in $[Ru(tpy)_2]^{2+}$ and $[Ru(bpy)_3]^{2+}$ that allow efficient tunnelling into high-lying singlet states.[77,83,91,120]

Decay path **E**: phosphoresence.

In the following, we will divide the discussion into tris(bidentate) complexes with $[Ru(N^N)_2(N^C)]^+$ coordination sphere and bis(tridentate) complexes with either $[Ru(N^N^N)(N^C^N)]^+$ or $[Ru(N^N^N)(N^N^C)]^+$ motifs to highlight similarities and differences between the different classes. Finally, we will suggest strategies how to improve the room temperature emission of such complexes and how our conclusions might impact the photophysics of cyclometalated polypyridine complexes of still elusive iron(II) emitters[6,121–123] and well-known iridium(III) emitters[49,104,124] as well.

Tris(bidentate) ruthenium complexes

The first cyclometalated (polypyridine)ruthenium complex, $[Ru(bpy)_2(ppy\text{-}NO_2)]^+$ $[\mathbf{1a}]^+$ (Hppy = 2-phenylpyridine, R^2 = NO_2), was reported in 1985 by Reveco *et al.* (Scheme 1).[125] Shortly thereafter, the syntheses of unsubstituted $[Ru(bpy)_2(ppy)]^+$ $[\mathbf{1b}]^+$[126] and the bis(tridentate) counterparts $[Ru(ttpy)(dpb)]^+$ (ttpy = 4′-*p*-tolyl-2,2′;6′,2″-terpyridine, dpbH = 1,3-di-(2′-pyridyl)benzene)[131] and $[Ru(tpy\text{-}4'\text{-}Cl)(pbpy)]^+$ (tpy = 2,2′;6′,2″-terpyridine, pbpyH = 6-phenyl-2,2′-bipyridine)[132] were

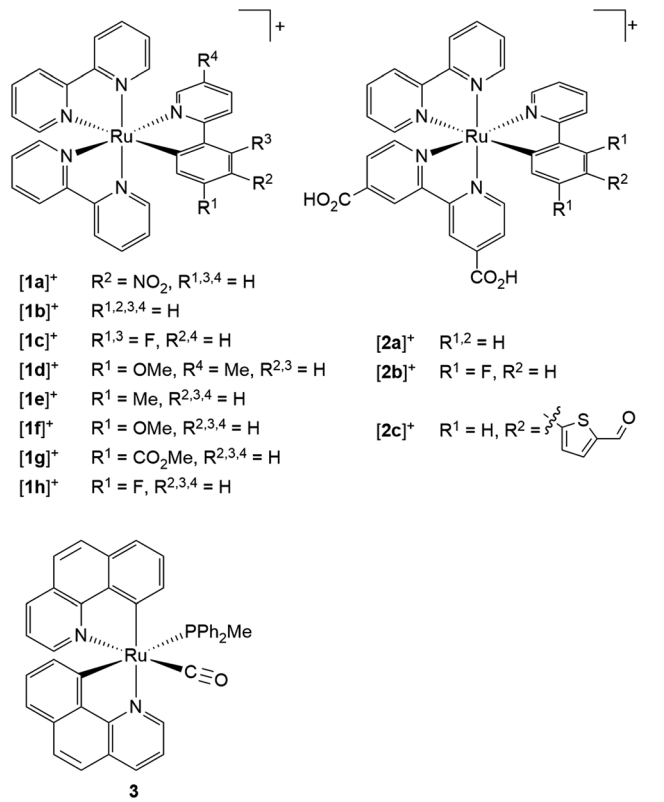

Scheme 1 Literature-known tris(bidentate) cyclometalated (polypyridine)ruthenium(II) complexes relevant to this work ($[\mathbf{1a}]^+$,[125] $[\mathbf{1b}]^+$,[126–128] $[\mathbf{1c}]^+$–$[\mathbf{1d}]^+$,[127] $[\mathbf{1e}]^+$–$[\mathbf{1h}]^+$,[128] $[\mathbf{2a}]^+$–$[\mathbf{2c}]^+$,[129] **3**[130]).

presented (*vide supra*). However, deeper interest in the photophysical properties of cyclometalated (polypyridine)ruthenium(II) complexes did not evolve until the discovery of their excellent performance as solar cell sensitizers in 2007.[16] Since then, more effort has been put into the understanding of the photophysical properties of this class of compounds.[107,109,117–119,127,133–135]

The visible range of the absorption spectrum of $[Ru(bpy)_2(ppy)]^+$-type complexes typically is dominated by two broad structured absorption bands, one appearing between 320 and 450 nm and the second between 470 and 650 nm.[107,127,133–135] The broadness of the visible range absorption features has been attributed to the low symmetry around the metal center which breaks the degeneracy of the metal's d orbitals. Additionally, the lowest unoccupied molecular orbital (LUMO) of the ppy unit (LUMO+2) is substantially higher in energy than the bpy LUMO (Fig. 2). Hence, Berlinguette and coworkers assigned these bands to Ru → ppy (at 400 nm) and Ru → bpy (at 500 nm) MLCT transitions.[3,107,127,135] Grätzel, however, suggested that all visible range absorption bands predominantly arise from Ru → bpy MLCT transitions with varying contributions from the highest occupied molecular orbital (HOMO) of π-symmetry at the cyclometalating phenyl ring.[17] Indeed, the theoretical data published by Berlinguette[107] show that all Ru → ppy transitions are weak in intensity and do not contribute to the absorption spectrum which supports Grätzel's interpretation. Additionally, the shift of the absorption bands induced by the functional groups attached to either the ppy ligand or the bpy units further underlines Grätzel's assignment of all bands as Ru → bpy transitions.[3,107,127,135]

For most tris(bidentate) complexes of this type, weak room temperature emission in the range between 720 and 820 nm is reported (Table 1).[107,127–129,133,135] The emissive state is considered to be a Ru → bpy ^{3}MLCT state.[107,133] This is corroborated by the influence of functional groups on the emission energy. In a series of $[Ru(bpy)_2(ppy\text{-}R)]^+$ complexes ([**1e**]$^+$–[**1h**]$^+$, Scheme 1) with functional groups in *meta*-position to the cyclometalating carbon atom, the emission energy decreases with increasing electron donating strength of the respective substituent as this destabilizes the metal d orbitals (Table 1).[128] Similarly, functionalization of the bpy ligands

Table 1 Emission wavelengths λ_{em} and wavenumbers $\tilde{\nu}_{em}$ as well as excited state lifetimes τ of selected tris(bidentate) cyclometalated (polypyridine)ruthenium(II) complexes at room temperature in solution

	λ_{em}/nm ($\tilde{\nu}_{em}$/cm^{-1})	τ/ns		λ_{em}/nm ($\tilde{\nu}_{em}$/cm^{-1})	τ/ns
[**1b**]$^+$ [127]	821 (12 180)	13	[**1g**]$^+$ [128]	781 (12 800)	—
[**1c**]$^+$ [127]	778 (12 850)	35	[**1h**]$^+$ [128]	776 (12 890)	—
[**1d**]$^+$ [127]	824 (12 140)	13	[**2a**]$^+$ [129]	787 (12 710)	9
[**1e**]$^+$ [128]	805 (12 420)	—	[**2b**]$^+$ [129]	761 (13 140)	27
[**1f**]$^+$ [128]	800 (12 500)	—	[**2c**]$^+$ [129]	779 (12 840)	14

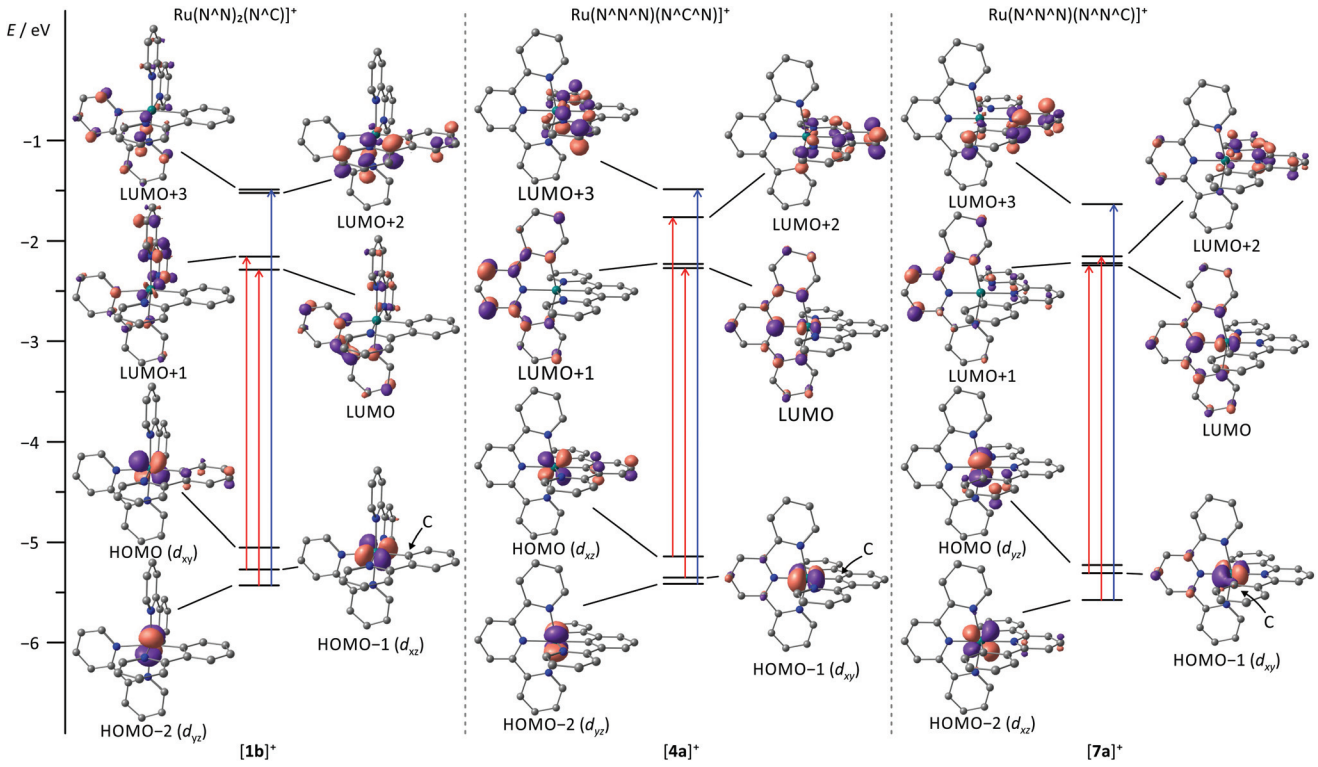

Fig. 2 MO diagram of the parent cyclometalated (polypyridine)ruthenium(II) complexes [**1b**]$^+$, [**4a**]$^+$ and [**7a**]$^+$ obtained from DFT calculations (B3LYP, def2-SVP, ZORA, COSMO (acetonitrile) contour value: 0.07). H atoms are omitted for clarity. The most important orbitals involved in the dominant transitions around 500 nm and 400 nm are highlighted in red and blue, respectively.

with electron accepting substituents such as COOR groups shifts the emission bathochromically as a consequence of the lowered LUMO energy (Table 1).[133] However, missing low-temperature emission data (λ_{em}, ϕ, τ) currently impede a quantification of the respective effects.

To the best of our knowledge, no quantum yields have been determined neither at room temperature nor at 77 K for any of the reported tris(bidentate) cyclometalated complexes due to their very weakly emissive character and the associated instrumental limitations.[127,128] Castellano and coworkers estimated the phosphorescence quantum yields to be $\phi < 0.005$,[127] while Housecroft and coworkers reported yields below 0.01 for compounds [**1e**]$^+$–[**1h**]$^+$.[128] However, Berlinguette[129] and Castellano[127] provided lifetime data of the emissive excited states for two series of complexes [**2a**]$^+$–[**2c**]$^+$ and [**1b**]$^+$–[**1d**]$^+$, respectively (Scheme 1, Table 1). The lifetimes are in the nanosecond range for all complexes and correlate nicely with the emission energy: the excited state lifetimes become smaller with decreasing emission energy. In (polypyridine)ruthenium(II) complexes, the emissive ^{3}MLCT state typically is depopulated to some extent *via* a ^{3}MC state (path **B**, *vide supra*).[84,89–91] However, cyclometalation substantially increases the ^{3}MC energy, as pointed out by Dixon[136] and van Koten,[137] efficiently retarding emission quenching *via* this pathway.[118] In fact, we were able to localize the respective ^{3}MLCT and ^{3}MC states of [**1b**]$^+$ *via* DFT calculations (Fig. 3). The ^{3}MC state (Mulliken spin population at Ru: 1.87) is located 66 kJ mol^{-1} above the ^{3}MLCT level while for [Ru(bpy)$_3$]$^{2+}$, the ^{3}MLCT-^{3}MC energy gap was calculated to be −7.7 kJ mol^{-1} in favour of the ^{3}MC state.[138–140] Remarkably, the nitrogen donor atom N1 of the cyclometalating ligand as well as the *trans* nitrogen atom N4 are essentially decoordinated in the ^{3}MC state of [**1b**]$^+$ with Ru–N distances of 2.48 and 2.39 Å, respectively (Fig. 4). This tetragonal distortion along the N1–Ru–N4 axis underlines the strongly dissociative character of the ^{3}MC state similar to that described for biscyclometalated tris(bidentate) iridium complexes[141–143] and for [Ru(bpy)$_3$]$^{2+}$.[138–140] It resembles the Jahn–Teller mode of d^7 low-spin Co^{II} complexes due to the $(e_g^*)^1$ electron configuration.[144,145]

The transition state between the ^{3}MC and ^{3}MLCT state was localized on the potential surface with an energy of 69 kJ mol^{-1} above the ^{3}MLCT state (Fig. 3). Hence, in contrast to the isoelectronic complex [Ru(bpy)$_3$]$^{2+}$, the ^{3}MC state of [**1b**]$^+$ is thermally inaccessible. The comparably low quantum yields of [**1b**]$^+$ are attributed to an increased thermal relaxation into the ground state. Non-emissive excited state decay occurs *via* vibronic coupling to high-energy oscillators (path **A**) or *via* a thermally activated surface crossing to the ground state potential surface (path **C**).[86] The latter requires a low-energy surface crossing point. We attempted to localize such a minimum energy crossing point (MECP) between the ^{3}MLCT and ^{1}GS potential surfaces. However, the lowest ^{3}MLCT → ^{1}GS MECP we could find was localized at 120 kJ mol^{-1} above the ^{3}MLCT level. An analogous ^{3}MC → ^{1}GS MECP on the other hand is localized at 72 kJ mol^{-1} merely 6 kJ mol^{-1} above the ^{3}MC state (path **B**, Fig. 3). However, since all of these states are thermally

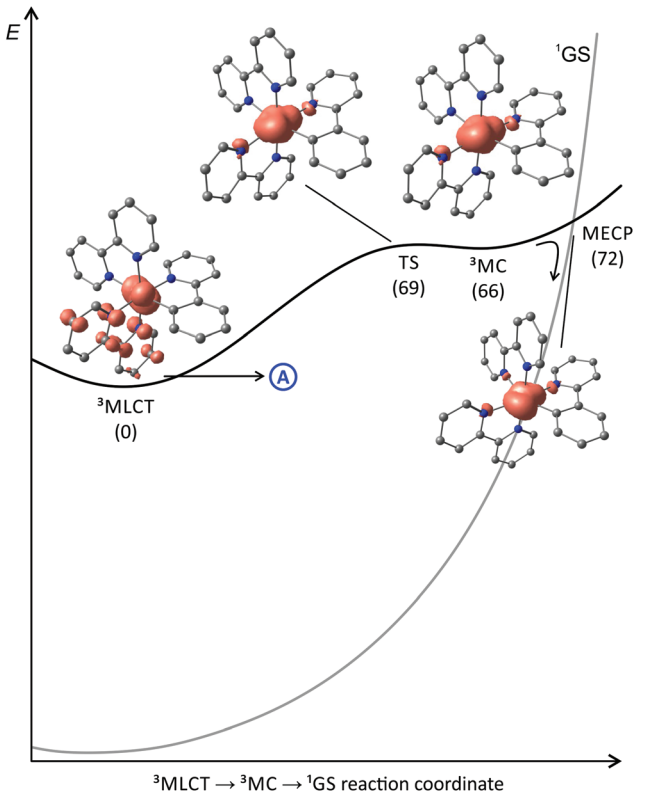

Fig. 3 Schematic representation of the energy landscape of [**1b**]$^+$ including spin density contour plots (contour value: 0.01) of the ^{3}MLCT and the ^{3}MC states as well as the ^{3}MLCT → ^{3}MC transition state and the ^{3}MC → ^{1}GS minimum energy surface crossing point. H atoms are omitted for clarity. Energies (kJ mol^{-1}) are given in parentheses relative to the ^{3}MLCT state (E = 0 kJ mol^{-1}). The shape of the singlet potential energy surface is estimated from the DFT-calculated triplet–singlet energy differences at the various excited state geometries.

inaccessible at room temperature or below, surface crossing to the singlet ground state is irrelevant for the excited state deactivation of [**1b**]$^+$. As a consequence, emission quenching in [**1b**]$^+$ appears to occur exclusively *via* tunnelling into high-energy oscillators of the ground state (path **A**). According to the energy gap law, the vibronic coupling of the ^{3}MLCT state and ^{1}GS becomes stronger, the smaller the ^{3}MLCT-^{1}GS energy gap is.[86–88] Secondly, a more pronounced distortion of the ^{3}MLCT excited state compared to the ground state geometry increases the non-radiative decay rate as it results in a higher Franck–Condon overlap of the vibronic wavefunctions of the ground and excited state.[86–88,127,146,147] Indeed, inspection of the DFT-optimized geometries of the ^{3}MLCT and ^{1}GS states reveals a sizable distortion of the former (Fig. 4) allowing for an efficient radiationless deactivation. This distortion is mainly localized at the bpy ligand *trans* to Ru–C. The Ru–N2 and Ru–N3 bonds are significantly elongated as a consequence of the formal oxidation of ruthenium to +III in the ^{3}MLCT state and the *trans* influence of the cyclometalating phenyl ring. However, while the Ru–N2 and Ru–N3 bonds are elongated, the formal negative charge on the second bpy ligand

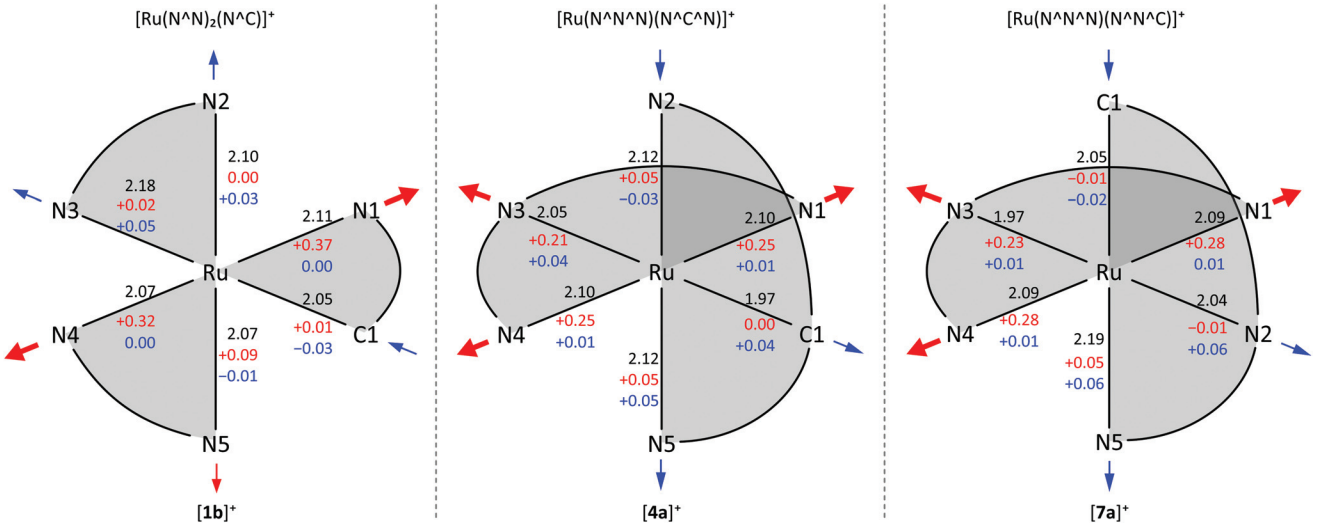

Fig. 4 Schematic representation of the ^{1}GS geometries of $[\mathbf{1b}]^+$, $[\mathbf{4a}]^+$ and $[\mathbf{7a}]^+$ including Ru–X bond lengths in Å (black). The bond length changes in Å in the ^{3}MC (red) and ^{3}MLCT states (blue) are given with respect to the ^{1}GS state. Arrows indicate major molecular distortions of the respective states.

compensates the repulsion yielding essentially unaltered Ru–N4 and Ru–N5 bond lengths.

In summary, the high energy of the ^{3}MC state is very favourable for efficient emitters because it eliminates one pathway for exited state deactivation and concomitantly prevents photodecomposition reactions, that typically occur from the dissociative ^{3}MC state.[90,148] However, in order to increase phosphorescence quantum yields of cyclometalated (polypyridine)ruthenium, radiationless deactivation *via* vibronic coupling has to be suppressed. This can be approached in two ways: the distortion of the ^{3}MLCT state compared to the ^{1}GS has to be reduced and the emission energy has to be blue-shifted as far as possible. Chou and coworkers provided a beautiful example successfully implementing both approaches.[130] Clever molecular design yielded systems with Ru → ppy MLCT states as lowest triplet excited states. This is straight-forwardly accomplished by making the cyclometalating ppy$^-$ ligand the strongest π-acceptor in the complex. Chou and coworkers achieved this with carbon monoxide and phosphanes which are rather poor π-acceptors towards Ru^{II} in biscyclometalated complexes of the type Ru(bq)$_2$(CO)(PPh$_2$Me) **3** (bqH = benzo-[*h*]quinoline, Scheme 1).[130] As the LUMO of bq$^-$ is much higher in energy than that of bpy (Fig. 2), the emission from the corresponding Ru → bq ^{3}MLCT state is blue-shifted substantially to 575 nm with a quantum yield of ϕ = 0.24. Additionally, as the excited state involves a cyclometalating ligand, its distortion compared to the ground state geometry should be less pronounced as in complex $[\mathbf{1b}]^+$. Similar observations were made for the isoelectronic osmium complexes.[149]

These findings suggest that with careful choice of suitable, very weakly π-accepting polypyridine ligands, cyclometalated (polypyridine)ruthenium complexes with similar emission behaviour arising from high-energy Ru → ppy ^{3}MLCT states are accessible. Another way of improving the emission behaviour of cyclometalated (polypyridine)ruthenium complexes could be by introducing tridentate chelate ligands as this potentially supresses excited state distortions while maintaining the high energies of parasitic ^{3}MC states. This should yield nested states with poorer Franck–Condon overlap (weakly coupling limit) which reduces tunnelling processes into high-energy singlet states (path **A**). We will discuss the possibilities and consequences of bis(tridentate) coordination spheres on the phosphorescence properties of cyclometalated ruthenium complexes in the next section.

Bis(tridentate) ruthenium complexes

Considering cyclometalated bis(tridentate) complexes, a distinction between $[Ru(N^N^N)(N^C^N)]^+$ and $[Ru(N^N^N)(N^N^C)]^+$ coordination environments is reasonable. The next two sections will highlight similarities between the two classes of bis(tridentate) complexes as well as important differences and compare these findings to those concerning tris(bidentate) complexes (*vide supra*).

The $[Ru(N^N^N)(N^C^N)]^+$ coordination sphere

Similar to tris(bidentate) complexes, the visible range of the absorption spectrum of bis(tridentate) complexes with central cyclometalation is dominated by intense and broad absorption bands that have been assigned to MLCT transitions. Again, two bands are observed, one in the range of 350–450 nm and a second between 470 and 650 nm. Van Koten[137,150] and Berlinguette[107] assigned the high energy MLCT band to Ru → dpb transitions and the low-energy band to Ru → tpy excitations based on relative orbital energies of the lowest π*-orbitals of the respective ligands (Fig. 2). Schubert and coworkers[117,151] on the other hand assigned the low-energy band to mixed MLCT and ligand-to-ligand charge transfer (LL′CT) transitions

arising from a HOMO–LUMO transition while the blue absorption band was attributed to mixed MLCT/LL′CT and MC transitions. We examined several $[Ru(dpb\text{-}R^1)(tpy\text{-}R^2)]^+$ complexes and demonstrated experimentally (resonance Raman spectroscopy) and theoretically that the low energy absorption arises from both Ru → tpy and Ru → dpb excitations (Fig. 2).[118,152] Excitation into the tpy-centered LUMO is only possible from the HOMO−1, while the dpb-centered LUMO+2 can be reached from the HOMO as evidenced from time-dependent DFT calculations. Both excitations occur at very similar energy and contribute comparably to the absorption band at 500 nm. The higher energy absorption features result from MLCT transitions targeting the higher π* orbitals of the tpy ligand. In fact, a LL′CT transition as suggested by Schubert[117] is symmetry-forbidden as it involves two mutually perpendicular π orbitals. This symmetry argument will become important for the emission properties as well.

Weak emission is observed under ambient conditions for most bis(tridentate) complexes with central cyclometalation in the range between 700 and 800 nm while the parent $[Ru(tpy)_2]^{2+}$ complex is virtually non-emissive at room temperature.[107,109,118,119,137,151] Van Koten[137] and we[118,119] determined extremely low quantum yields in the range of 10^{-5} for complexes of type $[Ru(dpb\text{-}R^1)(tpy\text{-}R^2)]^+$. In contrast to the tris(bidentate) series, however, no excited state lifetimes were reported so far (Table 2). Our attempts to obtain lifetimes suggested that they are in the picosecond range.[119]

Van Koten[137] studied complexes of the type $[Ru(dpb\text{-}R^1)(tpy\text{-}R^2)]^+$ bearing carboxy-substituents on either or both ligands (Scheme 2, [**4a**]$^+$–[**4d**]$^+$). The effect of the functional groups on the respective emission energy (Table 2) points to a ^{3}MLCT emissive state. In fact, a COOR substituent at the tpy ligand ([**4b**]$^+$) leads to complexes that are non-emissive at room temperature due to its stabilizing influence on the tpy-centered LUMO. Since the phosphorescence quantum yields decrease with increasing emission wavelength following the energy gap law, van Koten suggested vibrational relaxation as main source of emission quenching.[137] We extended this study by also introducing electron-donating substituents such as NH_2 and NHCOMe to the dpb ligand (Scheme 2, [**5a**]$^+$–[**5c**]$^+$) and the tpy ligand ([**5d**]$^+$).[118,119] Using theoretical methods we showed, that the emissive state is in fact a ^{3}MLCT state. The two singly occupied orbitals (SOMOs) in this state correspond to the d_{xy} (HOMO−1) and the tpy LUMO, respectively (Fig. 2). No dpb ligand participation was observed. However, we localized a second charge transfer state with LL′CT character (dpb → tpy, HOMO → LUMO orbital parentage) on the triplet potential energy surface. The mutually perpendicular SOMOs make this state spectroscopically undetectable and non-emissive (dark state). As third type of triplet states, the ^{3}MC states were found (Fig. 5 and Table 3). While the ^{3}LL′CT state is essentially undistorted compared to the ground state with only a small displacement of ruthenium towards C1 and a concomitant elongation of the Ru–N3 bond, the ^{3}MLCT state exhibits substantial distortions within the tpy ligand. It is inclined with respect to the plane perpendicular to the dpb ligand by 12° (Fig. 5). At the same time the Ru–C and Ru–N5 bonds are slightly elongated while the Ru–N2 bond shortens (Fig. 4). In the ^{3}MC state on the other hand, the peripheral pyridine rings of the tpy ligand are tilted away from the metal center forming dihedral angles of about 11° with the central pyridine ring, respectively. Furthermore, the all Ru–N_{tpy} bonds Ru–N1, Ru–N3 and Ru–N4 are substantially elongated (Fig. 4) underlining the dissociative character of the ^{3}MC state.

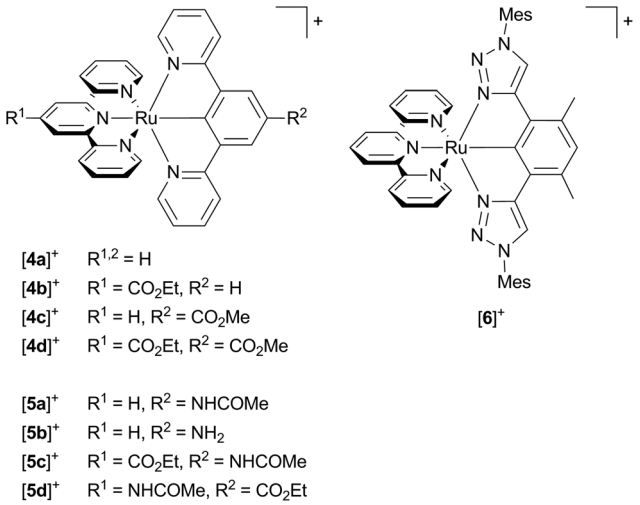

Scheme 2 Literature-known $[Ru(N^N^N)(N^C^N)]^+$ complexes relevant to this work ([**4a**]$^+$,[107,137] [**4b**]$^+$–[**4d**]$^+$,[137] [**5a**]$^+$ and [**5b**]$^+$,[119] [**5c**]$^+$ and [**5d**]$^+$,[118] [**6**]$^+$,[117]).

Table 2 Emission wavelengths λ_{em} and wavenumbers $\tilde{\nu}_{em}$ as well as quantum yields ϕ of selected $[Ru(N^N^N)(N^C^N)]^+$ complexes at room temperature

	λ_{em}/nm ($\tilde{\nu}_{em}$/cm^{-1})	ϕ
[**4a**]$^+$ [137]	781 (12 800)	9.4×10^{-6}
[**4b**]$^+$ [137]	—	—
[**4c**]$^+$ [137]	743 (13 460)	1.5×10^{-5}
[**4d**]$^+$ [137]	789 (12 670)	4×10^{-7}
[**5a**]$^+$ [119]	800 (12 500)	8×10^{-6}
[**5b**]$^+$ [119]	780 (12 820)	$<2 \times 10^{-6}$
[**5c**]$^+$ [118]	—	—
[**5d**]$^+$ [118]	751 (13 320)	1.4×10^{-5}
[**6**]$^+$ [117]	751 (13 320)	6.1×10^{-5}

The calculated relative energies of the triplet states (Fig. 5) of [**5a**]$^+$–[**5d**]$^+$ as well as the transition states connecting them are summarized in Table 3. The emissive ^{3}MLCT state is flanked by two thermally accessible quenching states, namely the ^{3}LL′CT and ^{3}MC states. The lowering of the relative ^{3}MC energy from 66 kJ mol^{-1} in [**1b**]$^+$ to 10–30 kJ mol^{-1} in these bis(tridentate) complexes is attributed to the smaller N–Ru–N bite angles and the weaker overlap of the nitrogen lone pairs with the e_g metal orbitals which results in a smaller ligand field splitting. The distortion of the ^{3}MC state allows for tunnelling to the ^{1}GS and for a surface crossing point (MECP) that is just 9 kJ mol^{-1} above the ^{3}MC level providing an accessible

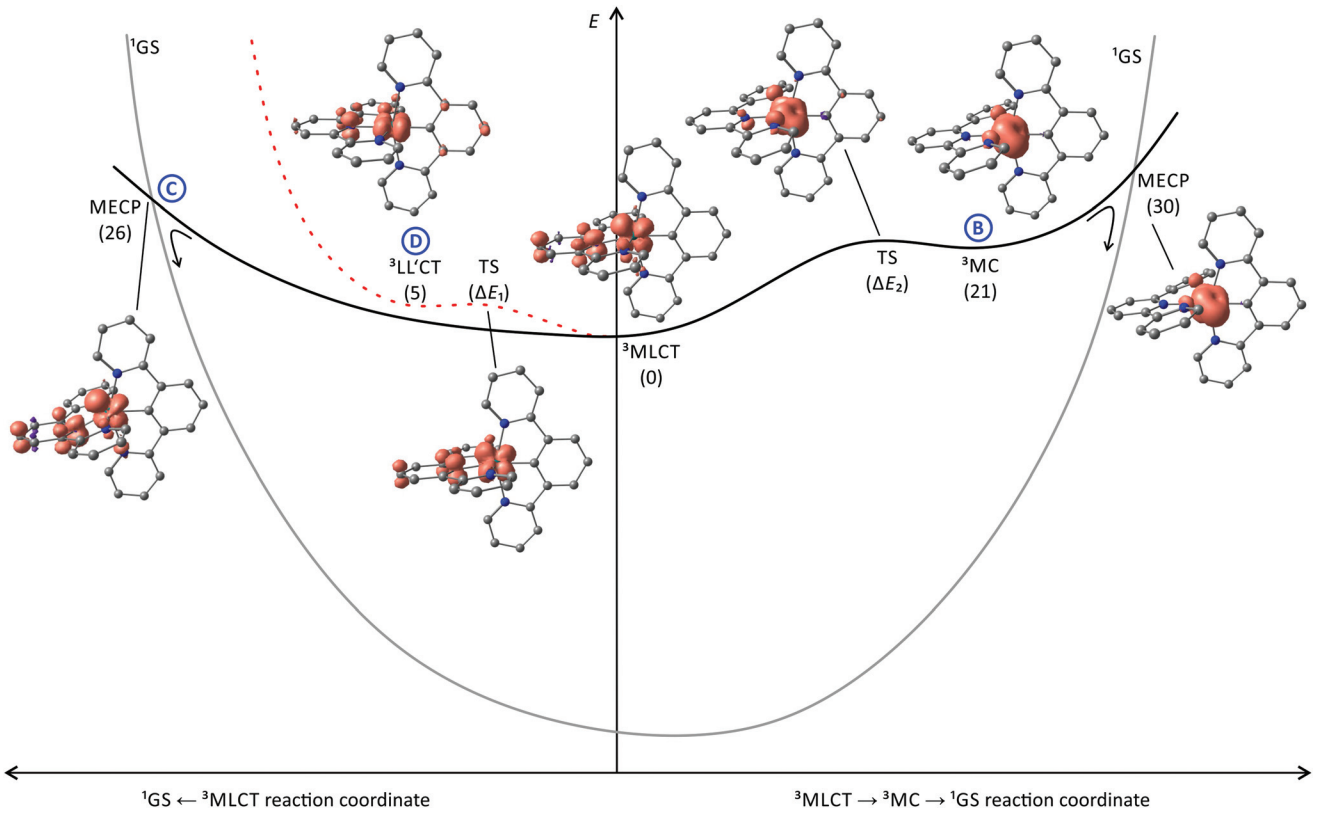

Fig. 5 Schematic representation of the energy landscape of $[Ru(dpb)(tpy)]^+$ type of complexes including spin density contour plots (contour value: 0.01) of the ^{3}LL′CT, ^{3}MLCT and ^{3}MC states of $[\mathbf{4a}]^+$, the ^{3}MLCT → ^{3}MC and ^{3}MLCT → ^{3}LL′CT transition states as well as the minimum energy points for the ^{3}MLCT → ^{1}GS and the ^{3}MC → ^{1}GS surface crossing. H atoms are omitted for clarity. Energies (kJ mol^{-1}) of the respective states are given in parentheses relative to the ^{3}MLCT state (E = 0 kJ mol^{-1}). The shape of the singlet potential energy surface is estimated from the DFT-calculated triplet–singlet energy differences at the various excited state geometries.

Table 3 DFT-calculated Gibbs free enthalpies (in kJ mol^{-1}) of the ^{3}LL′CT and ^{3}MC states as well as the ^{3}MLCT → ^{3}LL′CT (ΔE_1) and ^{3}MLCT → ^{3}MC (ΔE_2) transition states of complexes $[\mathbf{4a}]^+$, $[\mathbf{4c}]^+$, $[\mathbf{5a}]^+$, $[\mathbf{5b}]^+$, $[\mathbf{5d}]^+$ and $[\mathbf{6}]^+$ relative to the respective ^{3}MLCT state energy. Experimentally determined activation barriers are given in parentheses

	$E(^3\text{LL′CT})$	ΔE_1	$E(^3\text{MC})$	ΔE_2
$[\mathbf{4a}]^+$	5	5	21	23
$[\mathbf{4c}]^+$	−3	4 (2)	13	21 (22)
$[\mathbf{5a}]^+$	8	8 (6)	13	22 (23)
$[\mathbf{5c}]^+$	−10	—	31	—
$[\mathbf{5d}]^+$	—	—	9	(11)
$[\mathbf{6}]^+$	—	— (4)	—	— (22)

non-emissive deactivation channel for the ^{3}MLCT state (path **B**, Fig. 5).

Interestingly, a direct ^{3}MLCT → ^{1}GS MECP was found for $[\mathbf{4a}]^+$ as well at a moderate energy (26 kJ mol^{-1} above the ^{3}MLCT state). It is qualitatively similarly distorted as the ^{3}MLCT state but the degree of the distortion is larger. Thus, the geometry of this crossing point can be regarded as a high-amplitude distortional vibration along the ^{1}GS → ^{3}MLCT vibrational mode (^{3}MLCT → ^{1}GS reaction coordinate, Fig. 5). Hence, the ^{3}MLCT distortion of $[\mathbf{4a}]^+$ opens up this low-energy deactivation channel (path **C**), that is absent for $[\mathbf{1b}]^+$. However, experimental evidence for such a quenching channel is difficult to obtain as its activation barrier is similar to that of the ^{3}MC deactivation channel and hence a similar temperature-dependent emission behaviour is expected.

The ^{3}LL′CT state is connected to the ^{3}MLCT state *via* a transition state with a very low activation barrier (Table 3). As the ^{3}LL′CT state is barely distorted compared to the ^{1}GS geometry (*vide supra*) it is considered a nested state. Indeed, attempts to localize a ^{3}LL′CT → ^{1}GS MECP, that would provide a non-emissive decay channel, failed. Because emission from the ^{3}LL′CT state is symmetry-forbidden, its only decay pathway proceeds *via* tunnelling into the vibrationally excited singlet state followed by thermal relaxation (path **D**, Fig. 5).

Hence both, the ^{3}LL′CT and ^{3}MC states (and potentially also the ^{3}MLCT → ^{1}GS MECP) are responsible for the efficient phosphorescence quenching at room temperature. This DFT-based interpretation was evidenced experimentally by recording the temperature dependence of the quantum yield. The respective $\ln(\phi)$ *vs.* T^{-1} data of $[\mathbf{4c}]^+$ and $[\mathbf{5a}]^+$ were reproduced using a fit function accounting for two thermally activated de-

activation pathways. The activation barriers obtained from the fit are in excellent agreement with the computed transition state energies (Table 3).

Schubert and coworkers[117] published very similar results on structurally related complexes such as $[Ru(dtp)(tpy)]^+$ (dtbH = 1,3-di-(1,2,3-triazol-4-yl)benzene, Scheme 2, $[\mathbf{6}]^+$). Two Arrhenius-like activation parameters were required to properly reproduce the temperature-dependent lifetime data yielding very similar activation energies compared to our findings for $[\mathbf{4c}]^+$ and $[\mathbf{5a}]^+$. In contrast to our assignments, however, they attributed the two deactivation channels of $[\mathbf{6}]^+$ to an irreversible ^{3}MLCT → ^{3}MC surface crossing and an internal conversion to a higher-lying MLCT state of increased singlet character. The latter is a common feature of non-cyclometalated (polypyridine)ruthenium(II) complexes.[77,83,91,153] In the light of our results and the electronic similarity of the studied structures, it seems plausible that the second deactivation channel in $[\mathbf{6}]^+$ actually is *via* a state of ^{3}LL′CT nature as well. In fact, their DFT-optimization of a triplet state of $[\mathbf{6}]^+$ afforded a ^{3}CT state with orthogonal SOMOs.[117] Even if the cyclometalating ligand does not contribute significantly to the spin density of this state, its emissive relaxation is symmetry-forbidden.

To summarize, the combination of orthogonal ligands with strongly differing electronic properties, one being an excellent π-acceptor and the second a strong π-donor typically yields a low-lying ^{3}CT state. Even though this state is not directly populated after optical excitation into a ^{1}MLCT state and subsequent intersystem crossing onto the triplet manifold it serves as a further low-barrier channel for radiationless deactivation of the emissive ^{3}MLCT state (path **D**) besides the ^{3}MC state (path **B**). Recent reports underline that these results are transferable to structurally similar complexes of other transition metals with orthogonal tridentate ligands. In fact, Williams and coworkers suggested that a ^{3}LL′CT state plays a key role in the excited state deactivation of isostructural and isoelectronic $[Ir(N^N^N)(N^C^N)]^{2+}$ complexes.[154] A beautiful theoretical study on the excited state deactivation pathways in biscyclometalated gold(III) complexes of the general formula [Au(C^N^C)(acetylide)] revealed a ^{3}LL′CT state which efficiently contributed to the radiationless deactivation of the emissive state.[56,57,155] Its substantial distortion compared to the ground state increased the rate of non-radiative decay.

In order to optimize the emissive properties of bis(tridentate) cyclometalated ruthenium complexes, circumventing the low-energy non-emissive ^{3}LL′CT state is a key objective, for example by removing the axial symmetry. This can be achieved using a N^N^C coordination mode on the cyclometalating ligand which will be discussed in the next section (*vide infra*). However, the kinetic parameters extracted by Schubert and coworkers[117] from the temperature-dependent lifetime data suggest, that at room temperature the ^{3}LL′CT state (path **D**) with an activation barrier ΔE_2 of just 4.2 kJ mol^{-1} is only responsible for the quenching of about 25% of the excited molecules of $[\mathbf{6}]^+$ and structurally similar complexes. At the same time, the ^{3}MC state with a considerably higher barrier ΔE_1 of 21.9 kJ mol^{-1} is responsible for about 75% of the excited state deactivation (path **B** and potentially path **C**), while direct radiationless decay into the ground state only contributes 0.1% (path **A**). Hence, even avoiding the ^{3}LL′CT state by clever molecular design will not *per se* yield strong emitters. The strong electronic coupling of the ^{3}MLCT and ^{3}MC states [k_0 (^{3}MLCT → ^{3}MC) = 10^{11}–10^{13} s^{-1}; k_0 (^{3}MLCT → ^{3}LL′CT) ≈ 10^8 s^{-1}][117] renders the former the dominant deactivating state despite the substantially higher activation barrier. The appreciably weaker coupling of the ^{3}MLCT and ^{3}LL′CT states can be traced back to the two states still being electronically nearly orthogonal (*vide supra*). Concluding, despite the occurrence of a ^{3}LL′CT state in this kind of bis(tridentate) complexes the important states to manipulate for improving emission efficiencies remain the ^{3}MC and ^{3}MLCT states. Some well-thought-out examples have been provided in the recent literature employing ligand bite angle manipulation[94,95,156,157] and push–pull concepts[93,157,158] to increase the ^{3}MLCT-^{3}MC gap in bis(tridentate) ruthenium complexes which in principle are applicable to cyclometalated complexes as well. However, these conceptual approaches are beyond the scope of this perspective. Recently, Dixon and coworkers[159–161] suggested on a computational basis, that two cyclometalating sites in *cis*-position could be beneficial to increase the ligand field splitting of iron(II) complexes and provide a tool for controlling the relative ^{3}MLCT and ^{3}MC energies. This concept should be transferable to cyclometalated ruthenium complexes as well (*cf.* **3**) although it is likely accompanied with synthetic challenges.[105,130,162,163] An alternative approach could again involve attaching very weakly π-accepting ligands *trans* to a N^C^N ligand to yield potentially highly luminescent Ru → N^C^N ^{3}MLCT states.

The $[Ru(N^N^N)(N^N^C)]^+$ coordination sphere

The absorption spectrum of $[Ru(tpy)(pbpy)]^+$ type complexes resembles that of $[Ru(bpy)_2(ppy)]^+$ with two absorption bands, one around 400 nm, and a second around 500–600 nm. Again, the low-energy band is composed of MLCT transitions both involving the tpy and the cyclometalating ligand. However, the π* orbital of the coordinating phenyl ring (LUMO+3) is not involved in any of the low-energy transitions, as its energy is substantially higher than the frontier orbitals (Fig. 2).[107] Due to the near-degeneracy of the three lowest unoccupied orbitals (LUMO–LUMO+2), the absorption band at 500 nm is markedly sharper than that of $[Ru(dpb)(tpy)]^+$ and $[Ru(bpy)_2(ppy)]^+$ complexes. The feature around 400 nm is dominated by an intense Ru → phenyl (LUMO+3) transition (Fig. 2).[107]

Unfortunately, accounts on emission properties of these $[Ru(tpy)(pbpy)]^+$ complexes are very limited.[107,134,137,164] A few examples are summarized in Scheme 3 and Table 4. In the series $[\mathbf{7a}]^+$–$[\mathbf{7d}]^+$ with carboxy substituents at either or both ligands, the quantum yields and trends in the emission energies are similar to those of the isomeric $[Ru(tpy)(dpb)]^+$ complexes $[\mathbf{4a}]^+$–$[\mathbf{4d}]^+$. Again, carboxy-substitution at the tpy ligand lowers the LUMO energy sufficiently to yield non-emissive ($[\mathbf{7b}]^+$) or essentially non-emissive ($[\mathbf{7d}]^+$) complexes at room temperature due to the energy gap law.[137] However, carboxy-substitution at the pbpy ligand ($[\mathbf{7c}]^+$) does not blueshift the

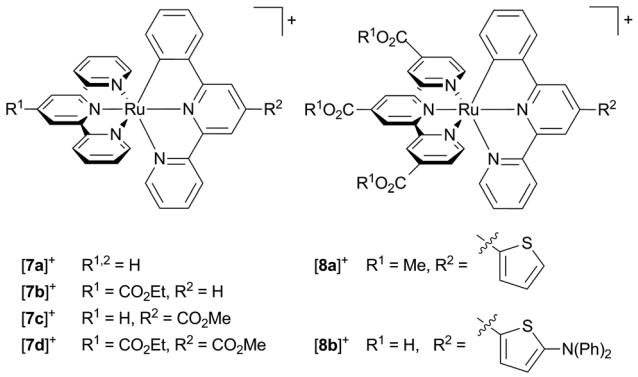

Scheme 3 Literature-known $[Ru(N^N^N)(N^N^C)]^+$ complexes relevant to this work ($[\mathbf{7a}]^+$–$[\mathbf{7d}]^+$,[107,137] $[\mathbf{8a}]^+$,[134] $[\mathbf{8b}]^+$ [164]).

Table 4 Emission wavelengths λ_{em} and wavenumbers $\tilde{\nu}_{em}$ as well as quantum yields ϕ of selected $[Ru(N^N^N)(N^N^C)]^+$ complexes at room temperature in solution

	λ_{em}/nm ($\tilde{\nu}_{em}$/cm^{-1})	ϕ
$[\mathbf{7a}]^+$ [137]	797 (12 550)	5.1×10^{-6}
$[\mathbf{7b}]^+$ [137]	—	—
$[\mathbf{7c}]^+$ [137]	780 (12 820)	1.3×10^{-5}
$[\mathbf{7d}]^+$ [137]	807 (12 390)	4×10^{-7}
$[\mathbf{8a}]^+$ [134]	810 (12 350)	—
$[\mathbf{8b}]^+$ [164]	549 (18 210)	0.27

emission energy compared to the unsubstituted complex $[\mathbf{7a}]^+$ (270 cm^{-1}) as much as in the case of the $[Ru(dpb)(tpy)]^+$ complexes $[\mathbf{4c}]^+$ and $[\mathbf{4a}]^+$ (660 cm^{-1}).[137] This was traced back to a change of the orbital parentage of the emissive ^{3}MLCT state. Instead of being a Ru → tpy state as in $[\mathbf{7a}]^+$, emission of $[\mathbf{7c}]^+$ arises from a Ru → (pbpy-COOR) ^{3}MLCT state. This is accompanied by an altered energy ordering of the lowest unoccupied orbitals and reflects their energetic similarity (Fig. 2). This example highlights that in $[Ru(N^N^N)(N^N^C)]^+$ type complexes Ru → N^N^C ^{3}MLCT states are obtained by tuning the respective frontier orbital energies of the ligands. However, the cyclometalating phenyl ring does not contribute as π-accepting moiety and the excited electron is entirely localized on the bipyridine fragment of the pbpy ligand. Consequently, the phosphorescence efficiency is not affected significantly (Table 4).

Interestingly, Berlinguette and coworkers reported on a series of $[Ru(tpy)(pbpy)]^+$ based complexes with diarylamine groups appended *via* a thiophene linker such as $[\mathbf{8b}]^+$. These are highly emissive (quantum yields in the range of 0.1–0.3) in some cases, but emit at much higher energy than typically observed for these complexes.[164] In fact, the analogous thiophene substituted complex $[\mathbf{8a}]^+$ without the diarylamine functionality lacks the strong emission.[134] However, Berlinguette showed that the emissive behaviour of $[\mathbf{8b}]^+$ actually arises from a singlet intraligand charge transfer state (^{1}ILCT) involving the diarylamine unit as electron donor and the polypyridine moiety as electron acceptor.[165,166] An identical emission energy was observed for the free ligand with even higher fluorescence quantum yields (ϕ = 0.91, τ = 3.4 ns) explaining the untypically high emission energy and quantum yield of $[\mathbf{8b}]^+$.[164–166]

To get a better understanding of the states involved in the excited state deactivation of $[Ru(tpy)(pbpy)]^+$ complexes, we studied the triplet potential energy surface of $[\mathbf{7a}]^+$ using DFT calculations. Inspecting the ^{3}MLCT state geometry and spin density of $[\mathbf{7a}]^+$ reveals a striking similarity to $[\mathbf{4a}]^+$ (Fig. 4, 5 and 6). In fact, a similar distortion of the tpy ligand with an offset central pyridine ring is found in both cases (*vide supra*). Additionally, the bond length changes of the ^{3}MLCT states compared to the respective ^{1}GS geometries of $[\mathbf{4a}]^+$ and $[\mathbf{7a}]^+$ are very similar (Fig. 4). Given the similar quantum yields of the isoelectronic classes of complexes $[Ru(dpb)(tpy)]^+$ and $[Ru(tpy)(pbpy)]^+$ this suggests excited state deactivation channels with similar barriers are dominant in both cases. However, the ^{3}MC state (path **B**) is found to be 60 kJ mol^{-1} (^{3}MLCT → ^{3}MC transition state at 62 kJ mol^{-1}) higher in energy than the ^{3}MLCT state and thus it is thermally inaccessible at room temperature. As a consequence, its contribution to the excited state deactivation of $[\mathbf{7a}]^+$ is negligible. The marked increase of the ^{3}MC-^{3}MLCT energy gap by about 30 kJ mol^{-1} by exchanging N^C^N by N^N^C chelate ligands in bis(tridentate) complexes (Fig. 6) was also found for the isoelectronic iron(II) complexes by Dixon and coworkers.[161] They argued that the cyclometalating ligand does not only act as a strong σ-donor but also as a π-donor. In the iron(II) complex $[Fe(dpb)(tpy)]^+$ the π-donor strength is the dominant influence yielding a net reduction of the effective ligand field strength and hence a stabilization of the ^{3}MC state compared to the non-cyclometalated complex $[Fe(tpy)_2]^{2+}$. In $[Fe(tpy)(pbpy)]^+$ on the other hand, the π-overlap between the peripheral cyclometalating phenyl ring and the metal d orbitals is not as pronounced. As a consequence of the σ-overlap an increased ligand field splitting and a higher ^{3}MC energy compared to $[Fe(dpb)(tpy)]^+$ are calculated. At the same time, the ^{3}MLCT energies of $[Fe(tpy)(pbpy)]^+$ and $[Fe(dpb)(tpy)]^+$ are essentially identical yielding an overall higher ^{3}MLCT-^{3}MC energy gap by about 30 kJ mol^{-1} for $[Fe(tpy)(pbpy)]^+$. As for ruthenium, the d orbitals are more diffuse than for iron, the destabilization of the t_{2g} orbitals *via* π-donor interactions is much less pronounced yielding ^{3}MC states well above the ^{3}MLCT level in all cyclometalating complexes, but the same principles apply explaining the trends we observe for the isoelectronic ruthenium complexes.[161]

In principle, a ^{3}LL′CT state similar to that described for $[Ru(dpb)(tpy)]^+$ complexes (*vide supra*) is also conceivable for complexes of the $[Ru(N^N^N)(N^N^C)]^+$ class. However, an analogous symmetry restriction as discussed above for the former does not apply in this case due to the lowered molecular symmetry. Although we tried to localize such a ^{3}LL′CT state it remained elusive. Whether such a state actually contributes to the excited state deactivation of $[Ru(N^N^N)(N^N^C)]^+$ complexes has to be evaluated based on experimental emission data at variable temperatures. This exceeds the scope of this article.

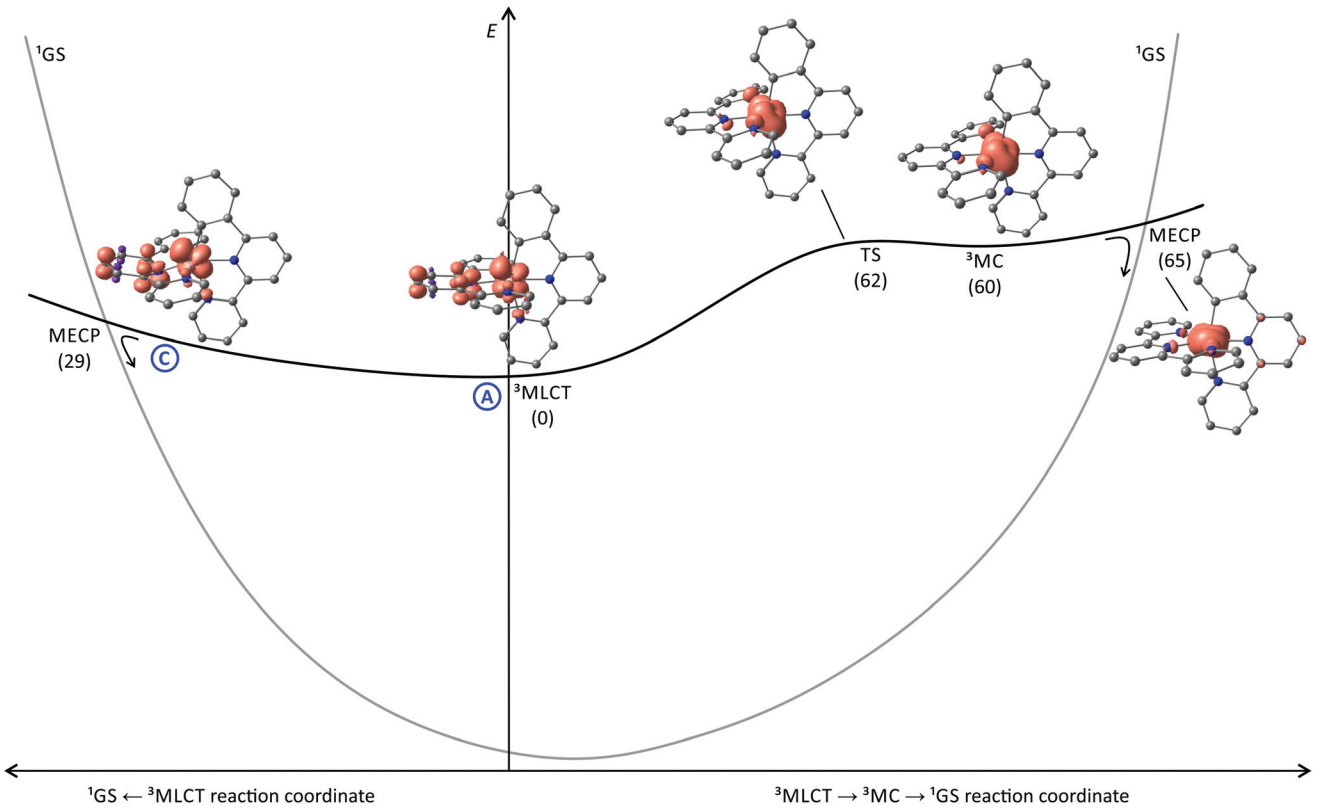

Fig. 6 Schematic representation of the energy landscape of $[Ru(tpy)(pbpy)]^+$ type of complexes including spin density contour plots (contour value: 0.01) of the ^{3}MLCT and ^{3}MC states of $[\mathbf{7a}]^+$, the ^{3}MLCT → ^{3}MC transition state as well as the minimum energy points for the ^{3}MLCT → ^{1}GS and the ^{3}MC → ^{1}GS surface crossing. H atoms are omitted for clarity. Energies (kJ mol^{-1}) of the respective states are given in parentheses relative to the ^{3}MLCT state (E = 0 kJ mol^{-1}). The shape of the singlet potential energy surface is estimated from the DFT-calculated triplet–singlet energy differences at the various excited state geometries.

Since the ^{3}MLCT state of $[\mathbf{7a}]^+$ is electronically very similar to the ^{3}MLCT state of the tris(bidentate) complex $[\mathbf{1b}]^+$, an argumentation based on emission quenching *via* vibronic coupling to the ground state (path **A**) is insufficient to account for the substantially lower emission quantum yields of the former (10^{-6}–10^{-5} as compared to 10^{-4}–10^{-3}). Additionally, deactivation channels *via* low-lying ^{3}MC (path **B**) or ^{3}LL′CT states (path **D**) as found for $[Ru(dpb)(tpy)]^+$ complexes do not contribute to the efficient non-emissive excited state decay of $[Ru(tpy)(pbpy)]^+$ complexes. A surface crossing point between the ^{3}MLCT and ^{1}GS potential energy surfaces (path **C**), however, similar to that found for $[\mathbf{4a}]^+$ (Fig. 5), would provide a concise explanation for the marked difference between the tris(bidentate) and bis(tridentate) complexes. Indeed, we localized a thermally accessible ^{3}MLCT → ^{1}GS surface crossing point that is only 29 kJ mol^{-1} higher in energy than the ^{3}MLCT state (Fig. 6). Remarkably, the geometry and energy of this crossing point is similar to that of the ^{3}MLCT → ^{1}GS MECP of $[\mathbf{4a}]^+$. Again, the distortion of the ^{3}MLCT state provides an excited state deactivation pathway for polypyridine ruthenium complexes. This finding has some predictive value as well. The ^{3}MC state is thermally inaccessible at temperatures below 298 K in $[\mathbf{7a}]^+$ and does not contribute to the excited state decay. Hence, the temperature dependence of the emission of $[\mathbf{7a}]^+$ can provide information on the contribution of a minimum energy surface crossing point in proximity to the relaxed ^{3}MLCT geometry to the emission quenching. An increasing emission intensity upon cooling would support this hypothesis. Additionally, as the dissociative anti-bonding ^{3}MC state is out of reach at room temperature, no photosubstitution reactions should occur for $[\mathbf{7a}]^+$ in contrast to $[Ru(bpy)_3]^{2+}$ which is very prone to such reactivity.[90] We will devote future work into elucidating these predictions.

In conclusion, it does not suffice to reduce the molecular symmetry and circumvent the parasitic ^{3}LL′CT state to increase phosphorescence quantum yields in bis(tridentate) cyclometalated complexes. Bis(tridentate) $[Ru(N^N^N)(N^N^C)]^+$ complexes with peripheral cyclometalation suffer from the same distortion and low energy of the ^{3}MLCT state as the analogous tris(bidentate) complexes. As the relative ^{3}MC state energy of $[Ru(tpy)(pbpy)]^+$ complexes is substantially higher than for comparable $[Ru(N^N^N)(N^C^N)]^+$ complexes, its contribution to the excited state decay can be neglected (path **B**). Hence, similar strategies are applicable for increasing the luminescence quantum yields as suggested before for tris(bidentate) complexes. These should focus on reducing the excited state distortion yielding a nested emissive state and shutting down the deactivation *via* direct ^{3}MLCT → ^{1}GS surface crossing

(path **C**). This might be achieved by shifting the LUMO to higher energies and making the π* orbital of the cyclometalating moiety the acceptor site of the lowest ^{3}MLCT state. At the same time, a lower excited state distortion would shift the energy of the ^{3}MLCT → ^{1}GS MECP to higher energies as well. This could potentially be accomplished by a combination of a very weakly π-accepting spectator ligand with a cyclometalating ligand that also contains a weakly π-accepting site such as an N-heterocyclic carbene.[167,168]

Experimental section

Density functional theory calculations

DFT calculations were carried out using the ORCA program package (version 3.0.2).[169] Tight convergence criteria were chosen for all calculations (Keywords TightSCF and TightOpt). All calculations were performed using the hybrid functional B3LYP[170] and employ the RIJCOSX approximation.[171,172] Relativistic effects were calculated at the zeroth order regular approximation (ZORA) level. The ZORA keyword automatically invokes relativistically adjusted basis sets.[173] To account for solvent effects, a conductor-like screening model (COSMO) modelling acetonitrile was used in all calculations.[174] Geometry, transition state and minimum energy crossing point optimizations were performed using Ahlrichs' split-valence double-ζ basis set def2-SV(P) which comprises polarization functions for all non-hydrogen atoms.[175,176] Optimized geometries were confirmed to be mimina or first-order saddle points by subsequent frequency analysis (n_{imag} = 0 or 1, respectively). Surface crossing geometries were subjected to SurfCrossNumFreq calculations to confirm that they are minima in the 3N–7 dimensional subspace excluding the surface crossing reaction coordinate. Computed free Gibbs enthalpies were used to compare the relative energies of all structures. Explicit counterions and/or solvent molecules were not taken into account in any case.

The ^{3}MLCT and ^{3}LL′CT states were localized by triplet geometry optimizations from the optimized ^{1}GS geometry. ^{3}MC states were found by elongating two opposite Ru–N bonds to 2.40 Å and subsequent geometry optimizations. Transition state optimizations were started from geometries obtained by averaging all coordinates of the starting and final state geometries using the exact Hessian matrix of the initial geometry. MECP geometries were obtained by starting at the respective optimized triplet state geometry (^{3}MLCT geometry for ^{3}MLCT-^{1}GS MECP, ^{3}MC geometry for ^{3}MC-^{1}GS MECP).

Conclusions

Cyclometalated polypyridineruthenium(II) complexes with N_5C coordination sphere typically exhibit very weak room temperature emission in the near infrared range (700–800 nm) of the electromagnetic spectrum. The reasons for the weak emission are various and depend on the chelate coordination sphere around the metal center. In tris(bidentate) $[Ru(N^N)_2(N^C)]^+$ complexes, the ^{3}MC state (path **B**) that is typically a major channel for excited state decay in polypyridineruthenium(II) complexes,[84,89,90] does not contribute as it is thermally inaccessible ($\Delta E(^3\text{MLCT} \rightarrow {}^3\text{MC})$ = 60–70 kJ mol^{-1}) at room temperature. Furthermore, no low energy ^{3}MLCT → ^{1}GS surface crossing point was found (path **C**) which suggests that tunnelling into high-energy vibrationally excited singlet states is the main channel of excited state deactivation (path **A**).

In contrast, the emission quenching of $[Ru(N^N^N)(N^C^N)]^+$ complexes is dominated by two thermally accessible triplet states, that flank the emissive ^{3}MLCT state, namely the ^{3}MC state (path **B**, $\Delta E(^3\text{MLCT} \rightarrow {}^3\text{MC})$ = 10–30 kJ mol^{-1}) and a ^{3}LL′CT state (path **D**, $\Delta E(^3\text{MLCT} \rightarrow {}^3\text{LL'CT})$ < 10 kJ mol^{-1}).[117–119] The ^{3}LL′CT state is a peculiarity of C_2-symmetric cyclometalated complexes and provides a second, unprecedented non-emissive deactivation channel. Additionally, a ^{3}MLCT → ^{1}GS surface crossing point provides another decay channel (path **C**) whose contribution yet needs to be quantified. These three channels **B**, **C** and **D** are responsible for almost 100% of the emission quenching. Although significantly faster than the emission process itself, direct non-emissive decay *via* ^{3}MLCT → ^{1}GS tunnelling (path **A**) only plays a subordinate role simply because excited state decay *via* paths **B**, **C** and **D** is so efficient. This is reflected by the very low excited state lifetimes below the nanosecond range.

In $[Ru(N^N^N)(N^N^C)]^+$ complexes, the ^{3}MC states are thermally inaccessible ($\Delta E(^3\text{MLCT} \rightarrow {}^3\text{MC}) \approx 60$ kJ mol^{-1}) and no quenching ^{3}LL′CT states are relevant. However, the triplet and singlet potential surfaces intersect close to the relaxed ^{3}MLCT state providing an efficient deactivation channel (path **C**) with an activation barrier of only about 30 kJ mol^{-1}. This explains the similarly low emission quantum yields of bis(tridentate) complexes with central and peripheral cyclometalating site despite the markedly different triplet states relevant to the two systems. However, the amount of emission quenching *via* tunneling (path **A**) in $[Ru(N^N^N)(N^N^C)]^+$ complexes remains unclear until temperature-dependent lifetime data are acquired.

Strategies for increasing the phosphorescence quantum yields are proposed. In $[Ru(N^N)_2(N^C)]^+$ complexes emission quenching is dominated the very low emission energies and the efficient tunnelling into high-energy singlet states following the energy gap law (path **A**). Hence, improving the emission efficiency is very challenging and only achieved by structurally restraining the already small excited state distortions or increasing the emission energy drastically. The latter is possible by making the cyclometalating ligand the π-accepting site of the ^{3}MLCT state as shown by Chou and coworkers.[130]

In bis(tridentate) cyclometalated ruthenium complexes, emission quenching predominantly arises from the distortion of the ^{3}MLCT state compared to the ground state. The triplet potential energy surface is relatively flat around the ^{3}MLCT geometry leading to a ^{3}MLCT/^{1}GS surface intersection less

than 30 kJ mol^{-1} above the emissive ^{3}MLCT state giving rise to a deactivation channel *via* a direct ^{3}MLCT → ^{1}GS surface crossing. Minimizing the excited state distortion *via* structural constraints could circumvent this channel. Additionally, by making the cyclometalating ligand the π-accepting site within the ^{3}MLCT state *via* tuning the energy levels of the lowest unoccupied molecular orbitals, a substantial increase of the ^{3}MLCT state energy can be achieved which would be beneficial for suppressing the ^{3}MLCT → ^{1}GS surface crossing as well. This will, however, also shift the emission well into the visible range of the electronic spectrum.

Furthermore, it is crucial to avoid orthogonal π-donor and π-acceptor sites in *trans* position across the metal center as in $[Ru(N^N^N)(N^C^N)]^+$ because this inherently invokes orthogonal, non-emissive ^{3}LL′CT states as quenching channels and also lowers the energy of the ^{3}MC states into a thermally accessible region due to a lower ligand field splitting.

In order to elucidate the excited state properties of cyclometalated complexes, temperature-dependent excited state lifetime or emission quantum yield measurements provide an invaluable tool.[71,117–119] Additionally, quantum chemical approaches can deliver lots of information about energies and geometries of relevant excited states. Tong, Che and coworkers (*vide supra*) demonstrated this on luminescent cyclometalated gold(III) complexes.[155] They assessed the radiative and non-radiative decay rates from a computational standpoint and quantified key processes that yield or prevent efficient emission in these species. Similarly, Dixon and coworkers studied mono- and bis(cyclometalated) iron(II) complexes using DFT calculations.[159–161] The ^{3}MC state in $[Fe(pbpy)(tpy)]^+$ with peripheral cyclometalation is substantially higher in energy than in $[Fe(dpb)(tpy)]^+$ with central cyclometalation, very similar to the results presented here for the ruthenium homologues. Furthermore, they highlighted, that bis(cyclometalated) iron(II) complexes such as [Fe(dpb)(pbpy)] and $[Fe(pbpy)_2]$ have very low-lying ^{3}MLCT states that are, in the case of [Fe(dpb)(pbpy)], only marginally distorted compared to the ground state geometry. We suggest that these findings apply to the analogous ruthenium complexes potentially opening a route to highly luminescent near-IR emitters. However, since only very few bis(cyclometalated) polypyridine ruthenium complexes are known so far[130,162,163] and none of them contain tridentate ligands, the synthesis of Ru(dpb)(pbpy) and $Ru(pbpy)_2$ complexes might be challenging. We will devote future work to the design and synthesis of ruthenium-based emitters with cyclometalating ligands to improve and exploit their excited state properties.

Acknowledgements

Parts of this research were conducted using the supercomputer MOGON and advisory services offered by Johannes Gutenberg Univ. Mainz (http://www.hpc.uni-mainz.de), which is a member of the AHRP and the Gauss Alliance e.V. This work was financially supported by the Deutsche Forschungsgemeinschaft (GSC 266, Materials Science in Mainz, scholarship for C. K.).

References

1 N. Alonso-Vante, J.-F. Nierengarten and J.-P. Sauvage, *J. Chem. Soc., Dalton Trans.*, 1994, 1649–1654.
2 T. Bessho, E. C. Constable, M. Graetzel, A. Hernandez Redondo, C. E. Housecroft, W. Kylberg, M. K. Nazeeruddin, M. Neuburger and S. Schaffner, *Chem. Commun.*, 2008, 3717–3719.
3 C. E. Housecroft and E. C. Constable, *Chem. Soc. Rev.*, 2015, **44**, 8386–8398.
4 S. Ferrere and B. A. Gregg, *J. Am. Chem. Soc.*, 1998, **120**, 843–844.
5 S. Ferrere, *Chem. Mater.*, 2000, **12**, 1083–1089.
6 T. C. B. Harlang, Y. Liu, O. Gordivska, L. A. Fredin, C. S. Ponseca, P. Huang, P. Chábera, K. S. Kjaer, H. Mateos, J. Uhlig, R. Lomoth, R. Wallenberg, S. Styring, P. Persson, V. Sundström and K. Wärnmark, *Nat. Chem.*, 2015, **7**, 883–889.
7 G. Sauvé, M. E. Cass, S. J. Doig, I. Lauermann, K. Pomykal and N. S. Lewis, *J. Phys. Chem. B*, 2000, **104**, 3488–3491.
8 T. Kinoshita, J.-i. Fujisawa, J. Nakazaki, S. Uchida, T. Kubo and H. Segawa, *J. Phys. Chem. Lett.*, 2012, 394–398.
9 E. I. Mayo, K. Kilså, T. Tirrell, P. I. Djurovich, A. Tamayo, M. E. Thompson, N. S. Lewis and H. B. Gray, *Photochem. Photobiol. Sci.*, 2006, **5**, 871–873.
10 E. Baranoff, J. Yum, I. Jung, R. Vulcano, M. Grätzel and M. K. Nazeeruddin, *Chem. – Asian J.*, 2010, **5**, 496–499.
11 B. O'Regan and M. Grätzel, *Nature*, 1991, **353**, 737–740.
12 M. K. Nazeeruddin, A. Kay, I. Rodicio, R. Humphry-Baker, E. Mueller, P. Liska, N. Vlachopoulos and M. Graetzel, *J. Am. Chem. Soc.*, 1993, **115**, 6382–6390.
13 M. K. Nazeeruddin, S. M. Zakeeruddin, R. Humphry-Baker, M. Jirousek, P. Liska, N. Vlachopoulos, V. Shklover, C.-H. Fischer and M. Grätzel, *Inorg. Chem.*, 1999, **38**, 6298–6305.
14 M. K. Nazeeruddin, P. Péchy, T. Renouard, S. M. Zakeeruddin, R. Humphry-Baker, P. Comte, P. Liska, L. Cevey, E. Costa, V. Shklover, L. Spiccia, G. B. Deacon, C. A. Bignozzi and M. Grätzel, *J. Am. Chem. Soc.*, 2001, **123**, 1613–1624.
15 M. Grätzel, *J. Photochem. Photobiol., C*, 2003, **4**, 145–153.
16 S. H. Wadman, J. M. Kroon, K. Bakker, M. Lutz, A. L. Spek, G. P. M. van Klink and G. van Koten, *Chem. Commun.*, 2007, 1907–1909.
17 T. Bessho, E. Yoneda, J.-H. Yum, M. Guglielmi, I. Tavernelli, H. Imai, U. Rothlisberger, M. K. Nazeeruddin and M. Grätzel, *J. Am. Chem. Soc.*, 2009, **131**, 5930–5934.
18 A. Hagfeldt, G. Boschloo, L. Sun, L. Kloo and H. Pettersson, *Chem. Rev.*, 2010, **110**, 6595–6663.
19 P. G. Bomben, K. C. Robson, B. D. Koivisto and C. P. Berlinguette, *Coord. Chem. Rev.*, 2012, **256**, 1438–1450.

20 H. D. Abruna, A. Y. Teng, G. J. Samuels and T. J. Meyer, *J. Am. Chem. Soc.*, 1979, **101**, 6745–6746.
21 I. Okura and N. Kim-Thuan, *J. Mol. Catal.*, 1979, **5**, 311–314.
22 J.-M. Lehn and R. Ziessel, *Proc. Natl. Acad. Sci. U. S. A.*, 1982, **79**, 701–704.
23 J. Hawecker, J.-M. Lehn and R. Ziessel, *J. Chem. Soc., Chem. Commun.*, 1983, 536.
24 H. Ozawa, M. Haga and K. Sakai, *J. Am. Chem. Soc.*, 2006, **128**, 4926–4927.
25 S. Rau, B. Schäfer, D. Gleich, E. Anders, M. Rudolph, M. Friedrich, H. Görls, W. Henry and J. G. Vos, *Angew. Chem.*, 2006, **118**, 6361–6364, (*Angew. Chem., Int. Ed.*, 2006, **45**, 6215–6218).
26 A. Fihri, V. Artero, M. Razavet, C. Baffert, W. Leibl and M. Fontecave, *Angew. Chem.*, 2008, **120**, 574–577, (*Angew. Chem., Int. Ed.*, 2008, **47**, 564–567).
27 J. W. Tucker and C. R. J. Stephenson, *J. Org. Chem.*, 2012, **77**, 1617–1622.
28 J. W. Tucker, Y. Zhang, T. F. Jamison and C. R. J. Stephenson, *Angew. Chem.*, 2012, **124**, 4220–4223, (*Angew. Chem., Int. Ed.*, 2012, **51**, 4144–4147).
29 M. Majek and A. Jacobi von Wangelin, *Angew. Chem.*, 2013, **125**, 6033–6035, (*Angew. Chem., Int. Ed.*, 2013, **52**, 5919–5921).
30 S. Paria and O. Reiser, *ChemCatChem*, 2014, **6**, 2477–2483.
31 S. M. Stevenson, M. P. Shores and E. M. Ferreira, *Angew. Chem.*, 2015, **127**, 6606–6610, (*Angew. Chem., Int. Ed.*, 2015, **54**, 6506–6510).
32 V. Balzani and S. Campagna, *Top. Curr. Chem.*, 2007, **280**, 1–273.
33 V. Balzani and S. Campagna, *Top. Curr. Chem.*, 2007, **281**, 1–327.
34 J. P. Paris and W. W. Brandt, *J. Am. Chem. Soc.*, 1959, **81**, 5001–5002.
35 V. W.-W. Yam and K. M.-C. Wong, *Chem. Commun.*, 2011, **47**, 11579–11592.
36 H. Xiang, J. Cheng, X. Ma, X. Zhou and J. J. Chruma, *Chem. Soc. Rev.*, 2013, **42**, 6128–6185.
37 H. Xu, R. Chen, Q. Sun, W. Lai, Q. Su, W. Huang and X. Liu, *Chem. Soc. Rev.*, 2014, **43**, 3259–3302.
38 S. M. Fredericks, J. C. Luong and M. S. Wrighton, *J. Am. Chem. Soc.*, 1979, **101**, 7415–7417.
39 A. Juris, S. Campagna, I. Bidd, J. M. Lehn and R. Ziessel, *Inorg. Chem.*, 1988, **27**, 4007–4011.
40 R. A. Kirgan, B. P. Sullivan and D. P. Rillema, *Top. Curr. Chem.*, 2007, **281**, 45–100.
41 K. K.-W. Lo, M.-W. Louie and K. Y. Zhang, *Coord. Chem. Rev.*, 2010, **254**, 2603–2622.
42 J. N. Demas, E. W. Harris, C. M. Flynn and D. Diemente, *J. Am. Chem. Soc.*, 1975, **97**, 3838–3839.
43 C. Creutz, M. Chou, T. L. Netzel, M. Okumura and N. Sutin, *J. Am. Chem. Soc.*, 1980, **102**, 1309–1319.
44 J. P. Sauvage, J. P. Collin, J. C. Chambron, S. Guillerez, C. Coudret, V. Balzani, F. Barigelletti, L. de Cola and L. Flamigni, *Chem. Rev.*, 1994, **94**, 993–1019.
45 D. Kumaresan, K. Shankar, S. Vaidya and R. H. Schmehl, *Top. Curr. Chem.*, 2007, **281**, 101–142.
46 D. Carstens and G. Crosby, *J. Mol. Spectrosc.*, 1970, **34**, 113–135.
47 A. Zilian, U. Maeder, A. von Zelewski and H. U. Guedel, *J. Am. Chem. Soc.*, 1989, **111**, 3855–3859.
48 M. T. Indelli, C. Chiorboli and F. Scandola, *Top. Curr. Chem.*, 2007, **280**, 215–255.
49 K. A. King, P. J. Spellane and R. J. Watts, *J. Am. Chem. Soc.*, 1985, **107**, 1431–1432.
50 M. G. Colombo, A. Hauser and H. U. Guedel, *Inorg. Chem.*, 1993, **32**, 3088–3092.
51 L. Flamigni, A. Barbieri, C. Sabatini, B. Ventura and F. Barigelletti, *Top. Curr. Chem.*, 2007, **281**, 143–203.
52 F. Barigelletti, D. Sandrini, M. Maestri, V. Balzani, A. von Zelewsky, L. Chassot, P. Jolliet and U. Maeder, *Inorg. Chem.*, 1988, **27**, 3644–3647.
53 H.-K. Yip, L.-K. Cheng, K.-K. Cheung and C.-M. Che, *J. Chem. Soc., Dalton Trans.*, 1993, 2933–2938.
54 D. R. McMillin and J. J. Moore, *Coord. Chem. Rev.*, 2002, **229**, 113–121.
55 J. A. G. Williams, *Top. Curr. Chem.*, 2007, **281**, 205–268.
56 W. H. Lam, E. S.-H. Lam and V. W.-W. Yam, *J. Am. Chem. Soc.*, 2013, **135**, 15135–15143.
57 E. S.-H. Lam, W. H. Lam and V. W.-W. Yam, *Inorg. Chem.*, 2015, **54**, 3624–3630.
58 V. W.-W. Yam and E. C.-C. Cheng, *Top. Curr. Chem.*, 2007, **281**, 269–309.
59 C. Bronner and O. S. Wenger, *Dalton Trans.*, 2011, **40**, 12409–12420.
60 N. A. P. Kane-Maguire and C. H. Langford, *J. Chem. Soc. D*, 1971, 895–896.
61 M. Maestri, F. Bolletta, L. Moggi, V. Balzani, M. S. Henry and M. Z. Hoffman, *J. Am. Chem. Soc.*, 1978, **100**, 2694–2701.
62 A. D. Kirk and G. B. Porter, *J. Phys. Chem.*, 1980, **84**, 887–891.
63 N. A. P. Kane-Maguire, *Top. Curr. Chem.*, 2007, **280**, 37–67.
64 S. Otto, M. Grabolle, C. Förster, C. Kreitner, U. Resch-Genger and K. Heinze, *Angew. Chem.*, 2015, **127**, 11735–11739, (*Angew. Chem., Int. Ed.*, 2015, **54**, 11572–11576).
65 A. Juris and R. Ziessel, *Inorg. Chim. Acta*, 1994, **225**, 251–254.
66 N. Armaroli, *Chem. Soc. Rev.*, 2001, **30**, 113–124.
67 N. Armaroli, G. Accorsi, F. Cardinali and A. Listorti, *Top. Curr. Chem.*, 2007, **280**, 69–115.
68 M. Iwamura, S. Takeuchi and T. Tahara, *Acc. Chem. Res.*, 2015, **48**, 782–791.
69 J. Nitsch, C. Kleeberg, R. Fröhlich and A. Steffen, *Dalton Trans.*, 2015, **44**, 6944–6960.
70 M. W. Mara, K. A. Fransted and L. X. Chen, *Coord. Chem. Rev.*, 2015, **282–283**, 2–18.
71 G. Capano, U. Rothlisberger, I. Tavernelli and T. J. Penfold, *J. Phys. Chem. A*, 2015, **119**, 7026–7037.
72 L.-Y. Zhang, G.-F. Liu, S.-L. Zheng, B.-H. Ye, X.-M. Zhang and X.-M. Chen, *Eur. J. Inorg. Chem.*, 2003, **2003**, 2965–2971.

73 K. Kalyanasundaram, *Coord. Chem. Rev.*, 1982, **46**, 159–244.
74 A. Juris, V. Balzani, F. Barigelletti, S. Campagna, P. Belser and A. von Zelewsky, *Coord. Chem. Rev.*, 1988, **84**, 85–277.
75 V. Balzani and A. Juris, *Coord. Chem. Rev.*, 2001, **211**, 97–115.
76 J. R. Winkler, T. L. Netzel, C. Creutz and N. Sutin, *J. Am. Chem. Soc.*, 1987, **109**, 2381–2392.
77 G. D. Hager and G. A. Crosby, *J. Am. Chem. Soc.*, 1975, **97**, 7031–7037.
78 T. J. Meyer, *Pure Appl. Chem.*, 1986, **58**, 1193–1206.
79 J. N. Demas and D. G. Taylor, *Inorg. Chem.*, 1979, **18**, 3177–3179.
80 S. Yoon, P. Kukura, C. M. Stuart and R. A. Mathies, *Mol. Phys.*, 2006, **104**, 1275–1282.
81 K. Suzuki, A. Kobayashi, S. Kaneko, K. Takehira, T. Yoshihara, H. Ishida, Y. Shiina, S. Oishi and S. Tobita, *Phys. Chem. Chem. Phys.*, 2009, **11**, 9850–9860.
82 G. A. Crosby, *Acc. Chem. Res.*, 1975, **8**, 231–238.
83 G. D. Hager, R. J. Watts and G. A. Crosby, *J. Am. Chem. Soc.*, 1975, **97**, 7037–7042.
84 J. van Houten and R. J. Watts, *J. Am. Chem. Soc.*, 1976, **98**, 4853–4858.
85 M. Kasha, *Discuss. Faraday Soc.*, 1950, **9**, 14–19.
86 R. Englman and J. Jortner, *Mol. Phys.*, 1970, **18**, 145–164.
87 J. V. Caspar, E. M. Kober, B. P. Sullivan and T. J. Meyer, *J. Am. Chem. Soc.*, 1982, **104**, 630–632.
88 J. V. Caspar and T. J. Meyer, *J. Phys. Chem.*, 1983, **87**, 952–957.
89 J. van Houten and R. J. Watts, *Inorg. Chem.*, 1978, **17**, 3381–3385.
90 B. Durham, J. V. Caspar, J. K. Nagle and T. J. Meyer, *J. Am. Chem. Soc.*, 1982, **104**, 4803–4810.
91 F. Barigelletti, A. Juris, V. Balzani, P. Belser and A. von Zelewsky, *Inorg. Chem.*, 1983, **22**, 3335–3339.
92 G. H. Allen, R. P. White, D. P. Rillema and T. J. Meyer, *J. Am. Chem. Soc.*, 1984, **106**, 2613–2620.
93 M. Maestri, N. Armaroli, V. Balzani, E. C. Constable and A. M. W. C. Thompson, *Inorg. Chem.*, 1995, **34**, 2759–2767.
94 M. Abrahamsson, M. Jäger, T. Österman, L. Eriksson, P. Persson, H.-C. Becker, O. Johansson and L. Hammarström, *J. Am. Chem. Soc.*, 2006, **128**, 12616–12617.
95 F. Schramm, V. Meded, H. Fliegl, K. Fink, O. Fuhr, Z. Qu, W. Klopper, S. Finn, T. E. Keyes and M. Ruben, *Inorg. Chem.*, 2009, **48**, 5677–5684.
96 A. Breivogel, C. Kreitner and K. Heinze, *Eur. J. Inorg. Chem.*, 2014, **2014**, 5468–5490.
97 R. D. Gerardi, N. W. Barnett and S. W. Lewis, *Anal. Chim. Acta*, 1999, **378**, 1–41.
98 S. Ji, W. Wu, W. Wu, P. Song, K. Han, Z. Wang, S. Liu, H. Guo and J. Zhao, *J. Mater. Chem.*, 2010, **20**, 1953–1963.
99 F. G. Gao and A. J. Bard, *J. Am. Chem. Soc.*, 2000, **122**, 7426–7427.
100 H. J. Bolink, L. Cappelli, E. Coronado and P. Gaviña, *Inorg. Chem.*, 2005, **44**, 5966–5968.
101 H. J. Bolink, L. Cappelli, E. Coronado, M. Grätzel and M. K. Nazeeruddin, *J. Am. Chem. Soc.*, 2006, **128**, 46–47.
102 H. J. Bolink, L. Cappelli, E. Coronado, M. Grätzel, E. Ortí, R. D. Costa, P. M. Viruela and M. K. Nazeeruddin, *J. Am. Chem. Soc.*, 2006, **128**, 14786–14787.
103 X. Yang, D. Neher, D. Hertel and T. K. Däubler, *Adv. Mater.*, 2004, **16**, 161–166.
104 M. S. Lowry and S. Bernhard, *Chem. – Eur. J.*, 2006, **12**, 7970–7977.
105 Y. Chi and P.-T. Chou, *Chem. Soc. Rev.*, 2010, **39**, 638–655.
106 C.-H. Yang, M. Mauro, F. Polo, S. Watanabe, I. Muenster, R. Fröhlich and L. de Cola, *Chem. Mater.*, 2012, **24**, 3684–3695.
107 P. G. Bomben, K. C. D. Robson, P. A. Sedach and C. P. Berlinguette, *Inorg. Chem.*, 2009, **48**, 9631–9643.
108 T. Funaki, H. Funakoshi, O. Kitao, N. Onozawa-Komatsuzaki, K. Kasuga, K. Sayama and H. Sugihara, *Angew. Chem.*, 2012, **124**, 7646–7649, (*Angew. Chem., Int. Ed.*, 2012, **51**, 7528–7531).
109 C. Kreitner, A. K. Mengel, T. K. Lee, W. Cho, K. Char, Y. S. Kang and K. Heinze, *Chem. – Eur. J.*, 2016.
110 M. Beley, J. P. Collin and J. P. Sauvage, *Inorg. Chem.*, 1993, **32**, 4539–4543.
111 C. Patoux, J.-P. Launay, M. Beley, S. Chodorowski-Kimmes, J.-P. Collin, S. James and J.-P. Sauvage, *J. Am. Chem. Soc.*, 1998, **120**, 3717–3725.
112 W.-W. Yang, J. Yao and Y.-W. Zhong, *Organometallics*, 2012, **31**, 1035–1041.
113 C.-J. Yao, R.-H. Zheng, Q. Shi, Y.-W. Zhong and J. Yao, *Chem. Commun.*, 2012, **48**, 5680–5682.
114 C.-J. Yao, H.-J. Nie, W.-W. Yang, J.-Y. Shao, J. Yao and Y.-W. Zhong, *Chem. – Eur. J.*, 2014, **20**, 17466–17477.
115 J.-J. Shen and Y.-W. Zhong, *Sci. Rep.*, 2015, **5**, 13835.
116 Y.-W. Zhong, Z.-L. Gong, J.-Y. Shao and J. Yao, *Coord. Chem. Rev.*, 2016, **312**, 22–40.
117 B. Schulze, D. Escudero, C. Friebe, R. Siebert, H. Görls, S. Sinn, M. Thomas, S. Mai, J. Popp, B. Dietzek, L. González and U. S. Schubert, *Chem. – Eur. J.*, 2012, **18**, 4010–4025.
118 C. Kreitner, E. Erdmann, W. W. Seidel and K. Heinze, *Inorg. Chem.*, 2015, **54**, 11088–11104.
119 C. Kreitner and K. Heinze, *Dalton Trans.*, 2016, **45**, 5640–5658.
120 A. C. Benniston, G. Chapman, A. Harriman, M. Mehrabi and C. A. Sams, *Inorg. Chem.*, 2004, **43**, 4227–4233.
121 L. A. Fredin, M. Pápai, E. Rozsályi, G. Vankó, K. Wärnmark, V. Sundström and P. Persson, *J. Phys. Chem. Lett.*, 2014, **5**, 2066–2071.
122 L. L. Jamula, A. M. Brown, D. Guo and J. K. McCusker, *Inorg. Chem.*, 2014, **53**, 15–17.
123 A. K. C. Mengel, C. Förster, A. Breivogel, K. Mack, J. R. Ochsmann, F. Laquai, V. Ksenofontov and K. Heinze, *Chem. – Eur. J.*, 2015, **21**, 704–714.
124 K. A. King and R. J. Watts, *J. Am. Chem. Soc.*, 1987, **109**, 1589–1590.

125 P. Reveco, J. H. Medley, A. R. Garber, N. S. Bhacca and J. Selbin, *Inorg. Chem.*, 1985, **24**, 1096–1099.
126 E. C. Constable and J. M. Holmes, *J. Organomet. Chem.*, 1986, **301**, 203–208.
127 M. L. Muro-Small, J. E. Yarnell, C. E. McCusker and F. N. Castellano, *Eur. J. Inorg. Chem.*, 2012, **2012**, 4004–4011.
128 C. D. Ertl, D. P. Ris, S. C. Meier, E. C. Constable, C. E. Housecroft, M. Neuburger and J. A. Zampese, *Dalton Trans.*, 2015, **44**, 1557–1570.
129 P. G. Bomben, K. D. Thériault and C. P. Berlinguette, *Eur. J. Inorg. Chem.*, 2011, **2011**, 1806–1814.
130 E. Y. Li, Y.-M. Cheng, C.-C. Hsu, P.-T. Chou, G.-H. Lee, I.-H. Lin, Y. Chi and C.-S. Liu, *Inorg. Chem.*, 2006, **45**, 8041–8051.
131 M. Beley, J. P. Collin, R. Louis, B. Metz and J. P. Sauvage, *J. Am. Chem. Soc.*, 1991, **113**, 8521–8522.
132 E. C. Constable, A. M. W. C. Thompson and S. Greulich, *J. Chem. Soc., Chem. Commun.*, 1993, 1444–1446.
133 P. G. Bomben, B. D. Koivisto and C. P. Berlinguette, *Inorg. Chem.*, 2010, **49**, 4960–4971.
134 H. Kisserwan, A. Kamar, T. Shoker and T. H. Ghaddar, *Dalton Trans.*, 2012, **41**, 10643–10651.
135 Z. Ji, G. Natu, Z. Huang, O. Kokhan, X. Zhang and Y. Wu, *J. Phys. Chem. C*, 2012, **116**, 16854–16863.
136 I. M. Dixon, F. Alary and J.-L. Heully, *Dalton Trans.*, 2010, **39**, 10959–10966.
137 S. H. Wadman, M. Lutz, D. M. Tooke, A. L. Spek, F. Hartl, R. W. A. Havenith, G. P. M. van Klink and G. van Koten, *Inorg. Chem.*, 2009, **48**, 1887–1900.
138 F. Alary, J.-L. Heully, L. Bijeire and P. Vicendo, *Inorg. Chem.*, 2007, **46**, 3154–3165.
139 J.-L. Heully, F. Alary and M. Boggio-Pasqua, *J. Chem. Phys.*, 2009, **131**, 184308.
140 T. Guillon, M. Boggio-Pasqua, F. Alary, J.-L. Heully, E. Lebon, P. Sutra and A. Igau, *Inorg. Chem.*, 2010, **49**, 8862–8872.
141 R. D. Costa, E. Ortí, D. Tordera, A. Pertegás, H. J. Bolink, S. Graber, C. E. Housecroft, L. Sachno, M. Neuburger and E. C. Constable, *Adv. Energy Mater.*, 2011, **1**, 282–290.
142 F. Monti, A. Baschieri, I. Gualandi, J. J. Serrano-Pérez, J. M. Junquera-Hernández, D. Tonelli, A. Mazzanti, S. Muzzioli, S. Stagni, C. Roldan-Carmona, A. Pertegás, H. J. Bolink, E. Ortí, L. Sambri and N. Armaroli, *Inorg. Chem.*, 2014, **53**, 7709–7721.
143 S. Yi, J.-H. Kim, Y.-J. Cho, J. Lee, T.-S. Choi, D. W. Cho, C. Pac, W.-S. Han, H.-J. Son and S. O. Kang, *Inorg. Chem.*, 2016, **55**, 3324–3331.
144 I. Krivokapic, M. Zerara, M. L. Daku, A. Vargas, C. Enachescu, C. Ambrus, P. Tregenna-Piggott, N. Amstutz, E. Krausz and A. Hauser, *Coord. Chem. Rev.*, 2007, **251**, 364–378.
145 R. G. Miller, S. Narayanaswamy, J. L. Tallon and S. Brooker, *New J. Chem.*, 2014, **38**, 1932–1941.
146 J. P. Claude and T. J. Meyer, *J. Phys. Chem.*, 1995, **99**, 51–54.
147 N. H. Damrauer, T. R. Boussie, M. Devenney and J. K. McCusker, *J. Am. Chem. Soc.*, 1997, **119**, 8253–8268.
148 J. V. Caspar and T. J. Meyer, *J. Am. Chem. Soc.*, 1983, **105**, 5583–5590.
149 K.-C. Hwang, J.-L. Chen, Y. Chi, C.-W. Lin, Y.-M. Cheng, G.-H. Lee, P.-T. Chou, S.-Y. Lin and C.-F. Shu, *Inorg. Chem.*, 2008, **47**, 3307–3317.
150 S. H. Wadman, J. M. Kroon, K. Bakker, R. W. A. Havenith, G. P. M. van Klink and G. van Koten, *Organometallics*, 2010, **29**, 1569–1579.
151 B. Schulze, D. G. Brown, K. C. D. Robson, C. Friebe, M. Jäger, E. Birckner, C. P. Berlinguette and U. S. Schubert, *Chem. – Eur. J.*, 2013, **19**, 14171–14180.
152 C. Kreitner, M. Grabolle, U. Resch-Genger and K. Heinze, *Inorg. Chem.*, 2014, **53**, 12947–12961.
153 F. Barigelletti, P. Belser, A. von Zelewsky, A. Juris and V. Balzani, *J. Phys. Chem.*, 1985, **89**, 3680–3684.
154 A. J. Wilkinson, H. Puschmann, J. A. K. Howard, C. E. Foster and J. A. G. Williams, *Inorg. Chem.*, 2006, **45**, 8685–8699.
155 G. S. M. Tong, K. T. Chan, X. Chang and C.-M. Che, *Chem. Sci.*, 2015, **6**, 3026–3037.
156 A. Breivogel, C. Förster and K. Heinze, *Inorg. Chem.*, 2010, **49**, 7052–7056.
157 A. Breivogel, M. Meister, C. Förster, F. Laquai and K. Heinze, *Chem. – Eur. J.*, 2013, **19**, 13745–13760.
158 K. Heinze, K. Hempel and M. Beckmann, *Eur. J. Inorg. Chem.*, 2006, **2006**, 2040–2050.
159 I. M. Dixon, F. Alary, M. Boggio-Pasqua and J.-L. Heully, *Inorg. Chem.*, 2013, **52**, 13369–13374.
160 I. M. Dixon, S. Khan, F. Alary, M. Boggio-Pasqua and J.-L. Heully, *Dalton Trans.*, 2014, **43**, 15898–15905.
161 I. M. Dixon, F. Alary, M. Boggio-Pasqua and J.-L. Heully, *Dalton Trans.*, 2015, **44**, 13498–13503.
162 J. M. Patrick, A. H. White, M. I. Bruce, M. J. Beatson, D. C. St. Black, G. B. Deacon and N. C. Thomas, *J. Chem. Soc., Dalton Trans.*, 1983, 2121–2123.
163 M. I. Bruce, M. J. Liddell, G. N. Pain, M. A. Bennett and H. Neumann, *Inorg. Synth.*, 1989, **26**, 171–180.
164 K. C. D. Robson, B. D. Koivisto, A. Yella, B. Sporinova, M. K. Nazeeruddin, T. Baumgartner, M. Grätzel and C. P. Berlinguette, *Inorg. Chem.*, 2011, **50**, 5494–5508.
165 K. C. D. Robson, B. D. Koivisto, T. J. Gordon, T. Baumgartner and C. P. Berlinguette, *Inorg. Chem.*, 2010, **49**, 5335–5337.
166 K. C. D. Robson, B. Sporinova, B. D. Koivisto, E. Schott, D. G. Brown and C. P. Berlinguette, *Inorg. Chem.*, 2011, **50**, 6019–6028.
167 W. A. Herrmann and C. Köcher, *Angew. Chem.*, 1997, **109**, 2256–2282, (*Angew. Chem., Int. Ed. Engl.*, 1997, **36**, 2162–2187).
168 Y.-M. Zhang, J.-Y. Shao, C.-J. Yao and Y.-W. Zhong, *Dalton Trans.*, 2012, **41**, 9280–9282.
169 F. Neese, *WIREs Comput. Mol. Sci.*, 2012, **2**, 73–78.
170 A. D. Becke, *J. Chem. Phys.*, 1993, **98**, 5648–5652.

171 F. Neese, F. Wennmohs, A. Hansen and U. Becker, *Chem. Phys.*, 2009, **356**, 98–109.
172 R. Izsák and F. Neese, *J. Chem. Phys.*, 2011, **135**, 144105.
173 D. A. Pantazis, X.-Y. Chen, C. R. Landis and F. Neese, *J. Chem. Theory Comput.*, 2008, **4**, 908–919.
174 S. Sinnecker, A. Rajendran, A. Klamt, M. Diedenhofen and F. Neese, *J. Phys. Chem. A*, 2006, **110**, 2235–2245.
175 A. Schäfer, H. Horn and R. Ahlrichs, *J. Chem. Phys.*, 1992, **97**, 2571–2577.
176 A. Schäfer, C. Huber and R. Ahlrichs, *J. Chem. Phys.*, 1994, **100**, 5829–5835.